



Efficient conversion of sewage sludge into hydrochar by microwave-assisted hydrothermal carbonization



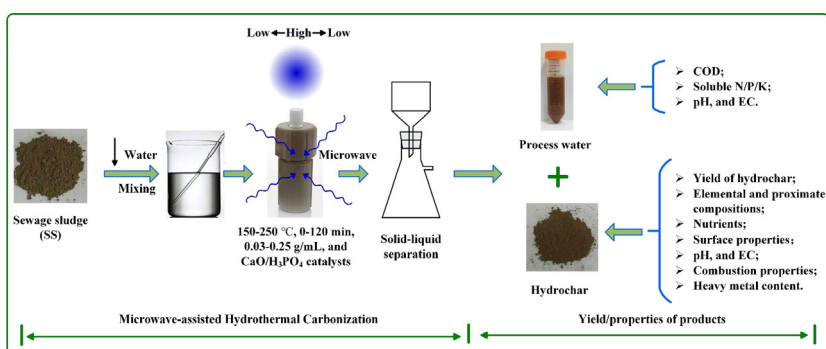
Yu-jie Wang, Yi Yu, Hua-jun Huang^{*}, Cheng-long Yu, Han-sun Fang, Chun-huo Zhou, Xin Yin, Wei-hua Chen, Xin-chun Guo^{*}

School of Land Resources and Environment, Key Laboratory of Agricultural Resource and Ecology in the Poyang Lake Basin of Jiangxi Province, Jiangxi Agricultural University, Nanchang 330045, PR China

HIGHLIGHTS

- Treatment of sewage sludge (SS) by microwave-assisted hydrothermal carbonization
- Hydrochar had higher aromaticity, porosity, and polarity than raw SS feedstock.
- Heavy metals and main nutrients (N/P/K) in hydrochars had a lower leaching/loss risk.
- Using CaO as a catalyst increased hydrochar yield and made it weakly alkaline.
- Using H₃PO₄ as a catalyst reduced hydrochar yield but promoted its burnout temperature.

GRAPHICAL ABSTRACT



ARTICLE INFO

Article history:

Received 14 June 2021

Received in revised form 12 August 2021

Accepted 20 August 2021

Available online xxxx

Editor: Daniel CW Tsang

Keywords:

Sewage sludge

Hydrothermal carbonization

Microwave

Hydrochar

Process water

ABSTRACT

The treatment of sewage sludge (SS) is an environmental problem worldwide. In recent years, hydrothermal carbonization (HTC) of SS for hydrochar (HC) has attracted extensive attention. This study preliminarily explored the microwave-assisted HTC of SS for the first time. Increasing the reaction temperature (150–250 °C) and reaction time (0–120 min) resulted in a decrease in the HC yield, and it gradually increased with the rising solid-liquid ratio (0.03–0.25 g/mL). Compared with raw SS, the HC products possessed higher aromaticity, carbonization degree, porosity, and polarity, and lower content of soluble nutrients (N/P/K) and leachable heavy metals (Cu, Zn, Pb, Cd, Cr, and Ni), indicating a lower risk of nutrient and heavy metal loss. Attention should be paid to the total contents of Zn and Cd in HC exceeded the permitted value for use in cultivated land with edible crops. The use of CaO as a catalyst improved the yield of HC, made the HC and process water (PW) weakly alkaline, and further passivated the heavy metals in the HC. In the case of H₃PO₄, although the conversion of SS was enhanced (lower content of volatile organic matter in HC), the contents of soluble nutrients (N/P/K) in HC/PW increased, and the migration of Zn and Cd into process water was enhanced. The HCs obtained in this study had poor combustion properties, but higher ignition temperatures than raw SS. PW must be properly treated or recycled because it still contained high contents of organic matter and nutrients. This fundamental study provides basic insights into the microwave-assisted HTC of SS.

© 2021 Elsevier B.V. All rights reserved.

^{*} Corresponding authors.

E-mail addresses: huanghuajun2004@126.com (H. Huang), 18807919339@139.com (X. Guo).

1. Introduction

Sewage sludge (SS), the main byproduct of municipal wastewater treatment plants (MWTPs), is produced in large amounts (Fu et al., 2021; Huang et al., 2017). The total estimated amount of SS generated in the European Union was 10.0 million tons (dry solids) in 2003–2006, and is expected to exceed 13.0 million by 2020 (Tarpani et al., 2020). According to the official statistics released by the Ministry of Housing and Urban-rural Development of China, in 2018, the number of MWTPs in China reached 2321, and the sewage treatment capacity reached 168.8 million m³/d. As a result, 11.8 million tons of dry SS were produced in China in 2018 (MOHURD of China, 2020). On the one hand, considering that SS contains much organic matter and rich nutrients, it is regarded as a potential resource. On the other hand, because of the many pathogens in SS and the accumulation of a certain amount of organic or inorganic pollutants, such as heavy metals, polycyclic aromatic hydrocarbons (PAHs), and polychlorinated biphenyls (PCBs), SS is also regarded as an environmental pollutant and requires proper treatment or disposal (Huang and Yuan, 2016; Xiao et al., 2020).

The prevalent SS disposal methods mainly include agricultural application to land, incineration, construction and building materials, and landfilling (Chang et al., 2020; Gao et al., 2020). However, these options are facing increasing challenges due to stringent environmental emission requirements and land restrictions (Manara and Zabaniotou, 2012). In recent years, thermochemical treatment of SS has been widely investigated in studies owing to resource recovery and utilization considerations; some examples of thermochemical treatment methods include pyrolysis, gasification, combustion, liquefaction, and hydrothermal carbonization (HTC) (Chanaka Udayanga et al., 2018; Huang and Yuan, 2015; Syed-Hassan et al., 2017). Thermochemical treatment processes generally require more complex equipment and procedures, but in general, they have higher efficiency, more evident volume reduction, and better economic performance (Gao et al., 2020). HTC is a promising thermochemical treatment for wet organic solid wastes (no prior drying is required) and is usually performed in water at relatively low temperatures (180–250 °C) and saturated pressures (2–10 MPa) with reaction time ranging from minutes to hours (Hämäläinen et al., 2021; Shen, 2020). After HTC treatment, the volume of SS is substantially reduced because of the enhancement of the dewaterability of SS. Meanwhile, SS is converted into high value-added products, that is, hydrochars (HCs), which have been widely applied in energy production, water remediation, soil amendment, and carbon sequestration (Tasca et al., 2019; Wang et al., 2019a).

Previous studies have primarily investigated six aspects regarding the HTC of SS: (i) the main process parameters, e.g., moisture content, temperature, residue time, catalyst, and heating rate, on the yield and properties of SS-derived hydrochar (Aragón-Briceño et al., 2020; Gaur et al., 2020; Yu et al., 2018; Zhang et al., 2021a). Reaction temperature is the most critical parameter affecting the reaction mechanism and product characteristics; (ii) the application of SS-derived HC in the purification of water pollutants, energy production, carbon sequestration, and soil improvement/remediation (Chu et al., 2020; Chung et al., 2017; Liu et al., 2021a; Ren et al., 2017; Tasca et al., 2020). The high ash content of SS-derived HC may be the main limiting factor for its use as an energy source and functional material; (iii) the fate and distribution of nutrients, PAHs, and heavy metals during the HTC of SS (Huang et al., 2018; Liu et al., 2018; Liu et al., 2021b; Wang et al., 2019b; Zhai et al., 2016; Zhang et al., 2018). HTC treatment has a certain degradation or passivation effect on pollutants and can effectively recover nutrient elements, especially phosphorus; (iv) the col-HTC of SS with fruit, agricultural and forestry wastes (He et al., 2019; Zhang et al., 2020a; Zhang et al., 2017). There is a synergistic effect between SS and other wastes to improve the efficiency of the entire HTC process; (v) the association of the HTC of SS with other processes (gasification, pyrolysis, and anaerobic digestion) (Gaur et al., 2020; Paneque et al., 2017; Wang et al., 2020d; Zheng et al., 2021). HTC can be used as an

efficient pretreatment technology for SS, which can effectively improve the efficiency of the subsequent treatment process; (vi) the comparison of the properties of SS-derived HC and SS-derived char produced by other processes (pyrolysis and gasification) or HC obtained from lignocellulosic biomass (Wang et al., 2021; Wilk et al., 2019; Zhang et al., 2021b). SS-derived HC shows some unique characteristics mainly caused by differences in the treatment process or material.

In recent years, microwave-assisted HTC of various types of biomasses has attracted extensive attention from researchers (Arpia et al., 2021; Nizamuddin et al., 2018; Sharma et al., 2020). Compared with traditional HTC (superficial/contact heating), microwave-assisted HTC (volumetric/non-content heating) often shows higher process efficiency (e.g., lower reaction time and energy consumption) and improved product yield and quality (Sharma et al., 2020). Microwave-assisted HTC has been applied to the treatment of lignocellulose (Elaiwu and Greenway, 2016; Kang et al., 2019; Knappe et al., 2018; Liu et al., 2021c; Shao et al., 2020), algae (Bach et al., 2017; Biller et al., 2013; Cao et al., 2019; Gan et al., 2020; Yu et al., 2020a), and livestock manure (Gao et al., 2018; Wang et al., 2020a). However, according to our review of the literature, research on the microwave-assisted HTC of SS has not been conducted. Because of differences in structure and composition between SS and the aforementioned biomass, further research on the microwave-assisted HTC of SS is particularly relevant and important.

CaO is usually used to improve acid soil; thus, the recovery and toxicity of CaO need not to be considered. CaO has been certified as a satisfactory catalyst in the HTC of swine manure (Lang et al., 2019b). H₃PO₄ has been shown to enhance the properties of HC obtained from the HTC of lignocellulose (rice straw, corn stover, and rape stalk) (Liu et al., 2021c). In this study, the microwave-assisted HTC of SS was systematically explored for the first time. First, the effects of the main process parameters (i.e., reaction temperature, reaction time, solid-liquid ratio, and catalyst [CaO and H₃PO₄]) on the yield of HC were investigated; next, the basic physicochemical properties of HC and process water (PW) were determined. This study aimed to provide a preliminary understanding of the microwave-assisted HTC of SS, namely, the selection of process parameters and the application potential of process products.

2. Materials and methods

2.1. Materials

The SS sample was obtained from a municipal wastewater treatment plant located in Nanchang City, Jiangxi Province, China. The moisture content of the original surplus sludge was about 99.2%, and after treatment in the sludge concentration tank, the water content was reduced to approximately 94.0%. The belt dehydrator was then used for mechanical dehydration, and the water content was reduced to approximately 77.0%. The SS after mechanical dewatering was collected as the experimental samples. The SS samples were firstly air-dried under natural conditions. To improve the control of the moisture content in the HTC process, the SS samples were further placed in an oven and dried at 105 °C for 12 h. Finally, the dried SS was crushed using a pulverizer, and the powder under 40 mesh was collected, placed in a self-sealing bag, and stored in a dryer for subsequent use. Ultra-pure water was used as the solvent in the microwave-assisted HTC of SS, and the two catalysts (calcium oxide and phosphoric acid) were analytically pure reagents. Calcium oxide (purity 99.9%) and phosphoric acid (purity higher than 85.0%) were purchased from Shenzhen Xilong Science Co., Ltd. and Shanghai Aladdin Biochemical Technology Co., Ltd., respectively.

2.2. Microwave-assisted HTC of SS

Microwave-assisted HTC experiments were performed using a microwave hydrothermal synthesis instrument (XH-8000Plus), designed and manufactured by Beijing Xianghu Technology Co., Ltd. (China).

The designed reaction temperature and pressure of the equipment were 260 °C and 6 MPa, respectively. The main procedures of the microwave-assisted HTC experiment were as follows: (i) according to the set solid-liquid ratio (R , 0.03–0.25 g/mL), a certain amount of SS was mixed with an appropriate amount of water, and the catalyst (if necessary, CaO [0–10 wt%] or H_3PO_4 [0–0.6 mol/L]) was added. The pH values of the reaction medium with and without the catalyst are shown in Table S1. After fully mixing, the mixture was transferred into a 100 mL microwave reaction kettle; (ii) the microwave reaction kettle was then sealed and transferred to a microwave hydrothermal synthesizer, and the pipeline was connected; (iii) the reaction kettle was heated up to the set reaction temperature (T , 150–250 °C), which was maintained for a certain reaction time (t , 0–120 min). During the reaction process, the reactants in the reaction kettle were stirred at 320 rpm. (iv) after the reaction was complete, a built-in fan was automatically turned on in order to cool the reaction kettle quickly. When the reaction kettle was cooled to room temperature, the reaction kettle was opened and the solid-liquid mixture was collected and separated using a vacuum filtration device.

The solid product, HC, was transferred to an oven and dried at 105 °C for 12 h, and then weighed to calculate its yield. After drying, the HC was placed in a self-sealing bag and stored in a dryer. The liquid product, PW, was transferred to a special plastic bottle and stored in a refrigerator for further analysis. The yield of HC (Y_1 , wt%) was determined according to Eq. (1).

$$Y_1 = \frac{m_{HC}}{m_{SS} + m_{catalyst}} \times 100 \quad (1)$$

where m_{HC} , m_{SS} , and $m_{catalyst}$ are the mass (g) of the HC, raw SS feedstock, and catalyst, respectively.

2.3. Chemical analysis of raw SS and HC

The pH and electrical conductivity (EC) of raw SS and HC were defined as the corresponding values of their respective leaching solutions at a solid/liquid ratio of 1:10 (g/mL), which were measured using a pH meter (HS-3C, INESA, China) and a conductivity meter (DDS-11A, INESA, China), respectively (Wang et al., 2020b). The contents of volatile organic matter (VOM) and ash in raw SS and HC were determined using a muffle furnace (SX2-2.5-10NP, Yiheng, China) according to previously reported methods (Pan et al., 2018). The difference between the 100 wt % and the total contents of VOM and ash (wt%) was defined as the content of fixed carbon (FC, wt%). The elemental compositions (C, H, and N, referring to the total content) of raw SS and HC were analyzed by an elemental analyzer (EL III, Elementar, Germany). A modified Dulong formula was applied to evaluate the calorific value (CV, MJ/kg) of raw SS and HCs (higher heating value), which is given in Eq. (2) (Hosokai et al., 2016; Huang et al., 2019).

$$CV = 0.382 \times C + 0.849 \times \left(H - \frac{O}{8} \right) \quad (2)$$

where C , H , and O are the percentages of carbon, hydrogen, and oxygen in the raw SS feedstock and HC, respectively (wt%).

Combustion experiments are a commonly used method to evaluate the combustion performance of a material, which can be realized by analyzing the thermochemical behavior of the material in the air atmosphere by using a thermogravimetric analyzer. Combustion experiments have been widely used to test the combustion performance of various HCs from livestock manure, lignocellulose, and SS (Lang et al., 2019c; Peng et al., 2016; Zhang et al., 2021c). In this study, a thermogravimetric analyzer (Discovery TGA55, TA Instruments-Waters, USA) was used to perform the combustion experiments of raw SS or HC. Approximately 10 mg of raw SS or HC was loaded into a platinum plate, which was then heated from 30 °C to 900 °C at a constant heating rate of 20 °C/min. During the combustion process, pure air was

introduced at a constant flow rate of 100 mL/min. According to the thermogravimetric (TG) and differential thermogravimetric (DTG) curves, four combustion parameters could be obtained, including the ignition temperature (T_i), burnout temperature (T_b), maximum weight loss rate (DTG_{max}), and mass residue (R_m). T_i was determined by using an extrapolation method based on the TG/DTG curves (Zhang et al., 2013). T_b was defined as the starting temperature when the weight loss rate was less than 1 wt%/min (Peng et al., 2016).

The comprehensive combustion index (CCI) and combustion stability index (CSI) were calculated using Eqs. (3) and (4) (Lang et al., 2019a).

$$CCI = \frac{DTG_{max} \times DTG_{mean}}{T_i^2 \times T_b} \quad (3)$$

$$CSI = \frac{DTG_{max}}{T_i \times T_m} \times 8.5875 \times 10^7 \quad (4)$$

where DTG_{mean} is the average weight loss rate, and T_m is the temperature corresponding to DTG_{max} .

The surface morphologies of the raw SS and HCs were determined by a scanning electron microscopy (Regulus 8100, Hitachi, Japan). A specific surface and porosity tester (JW-BK132F, JWGB, China) was used to detect the specific surface area, pore size, and pore volume of the HCs using the gas adsorptive method (N_2 adsorption-desorption isotherms). The total contents of heavy metals (Cu, Zn, Pb, Cd, Cr, and Ni) in raw SS and HCs were analyzed according to the mixed-acid digestion method (HNO_3 – H_2O_2 (30%)– $HClO_4$). Detailed digestion procedures have been described in the literature (Pan et al., 2019; Yang et al., 2017; Yuan et al., 2011). The leachable toxicity of the aforementioned six heavy metals was assessed according to the extraction procedure for leaching toxicity in solid waste using H_2SO_4 – HNO_3 as an extractant (Wang et al., 2020a). An inductively coupled plasma emission spectrometer (NexION 1000, PerkinElmer, USA) was used to detect the concentrations of the heavy metals in the corresponding digestion/extraction solution.

The contents of total phosphorus (TP) in the raw SS and HCs were determined in the light of the Mo–Sb anti spectrophotometric method (CJ/T 221–2005). For obtaining the TP concentrations, raw SS and HCs were melted with NaOH (heating to 400 °C and holding for 15 min and then further heating to 650 °C and holding for 15 min). The contents of total potassium (TK) in the raw SS and HCs were also detected using an inductively coupled plasma emission spectrometer (NexION 1000, PerkinElmer, USA) after initially digesting the raw SS and HCs with HNO_3 – H_2O_2 (30%)– HCl (CJ/T 221–2005). $NaHCO_3$ (0.5 mol/L, pH = 8.5, oscillating at 180 r/min for 30 min at room temperature [25 °C]) and NH_4OAC (1.0 mol/L, natural, oscillating at 180 r/min for 30 min at room temperature [25 °C]) were used as extractants for detecting soluble phosphorus (SP) and soluble potassium (SK), respectively. The concentration of SP in the extraction solution was detected by the same method used for TP, and the content of SK was determined using a flame photometer (FP 640, AOPU, China) (HJ 704–2014; NY/T 889–2004). The content of soluble nitrogen (SN) in raw SS and HCs was determined by the method of alkali hydrolysis diffusion (1.0 mol/L NaOH, 40 °C for 24 h) (Bao, 2000).

2.4. Chemical analysis of PW

The $K_2Cr_2O_7$ oxidation method was applied to analyze the organic matter content in PW in the form of chemical oxygen demand (COD). The pH and EC of the PW were measured using a pH meter (PHS-3C, INESA, China) and a conductivity meter (DDS-11A, INESA, China), respectively. The content of NH_4^+ -N in the PW was analyzed by the method of Nash's reagent colorimetry (HJ 535–2009). The concentrations of soluble phosphorus/potassium in the PW were directly detected

by the Mo—Sb anti spectrophotometric method and a flame photometer (FP 640, AOPU, China), respectively.

2.5. Statistical analysis of data

Each HTC experiment was conducted twice. The yield of HC was an average of the two experiments. When the deviation was above 5% between the two datasets, the experiment was repeated. The pH, EC, elemental, proximate, and nutrient compositions of HC and PW were also tested twice according to the general or standard test methods, and the corresponding average values were used. Other analyses, including specific surface analysis, thermogravimetric analysis, environmental scanning electron microscope analysis, and heavy metal content detection, were entrusted to a professional institution with official inspection and testing qualifications (Center of Analysis and Testing, Nanchang University), which can ensure the accuracy of inspection and test results.

3. Results and discussions

3.1. Influence of reaction temperature (T)

The effect of reaction temperature (T , 150–250 °C) on the formation of HC was explored during the microwave-assisted HTC of SS with a fixed reaction time (30 min) and solid–liquid ratio (0.03 g/mL) in the absence of any catalyst. As shown in Fig. 1(a), the yield of hydrochar continuously decreased with an increase in reaction temperature. The decrease was particularly evident for temperatures below 190 °C (by 11.84 wt%) and then weakened (only by 4.67 wt% at temperatures ranging from 190 °C to 250 °C). During the conventional HTC of SS, it was also found that increasing the reaction temperature resulted in a gradual decrease in the HC yield (Peng et al., 2016; Xu and Jiang, 2017). A similar phenomenon was also observed during the microwave-assisted HTC of corm stalk, pig feces, and red seaweed (Cao et al., 2019; Kang et al., 2019; Wang et al., 2020a). The key role of the reaction temperature was to provide sufficient heat to decompose organic macromolecules for the fragmentation and recombination of highly active chemical bonds. Therefore, hydrothermal reactions would become more active at higher temperatures, greatly accelerating the degradation and polymerization rate of SS compounds (Wang et al., 2019a). Particularly, the increase in reaction temperature promoted the decomposition and hydrolysis of macromolecular organic matter, as well as the hydrolysis of inorganic solid matter. Therefore, the content of VOM in HC gradually decreased with the increase in reaction temperature, and the EC of PW continuously increased from 0.89 ms/cm to 2.66 ms/cm (Fig. 1(a)).

3.2. Influence of reaction time (t)

The influence of reaction time (t , 0–120 min) was explored: the microwave-assisted HTC of SS was conducted at 230 °C with a fixed solid–liquid ratio (0.03 g/mL) in the absence of any catalyst. Fig. 1(b) shows the detailed results. When the reaction time was prolonged from 0 to 30 min, the yield of HC gradually decreased by 2.67 wt%. However, when the reaction time was extended to 60 min, the yield of HC was only slightly reduced by 0.83 wt%. Further increases in the reaction time resulted in no evident change in the yield of HC, and it fluctuated between 64.37 and 64.84 wt%. In other words, a reaction time of 30 min seemed to contribute to a significant solubilization/decomposition of SS components or a substantial conversion of SS. Elaigwu and Greenway (2016) conducted the microwave-assisted HTC of rapeseed husk and reported that the decrease in HC yield was rapid before 20 min and subsequently became almost stable. A longer reaction time usually means higher reaction intensity. Therefore, in a certain range of reaction time, increasing the reaction time would promote the degradation of organic components (as observed in the decrease in VOM in HCs) and the dissolution of inorganic components in SS (as observed in the increase in EC in PW) (Wang et al., 2020a). From the view of

industrialization, the shorter the reaction time is, the better it is to improve the process efficiency and save the process cost.

3.3. Influence of solid–liquid ratio (R)

The influence of the solid–liquid ratio (R , 0.03–0.25 g/mL) on the microwave-assisted HTC of SS was also investigated, which was performed at 230 °C with a fixed reaction time (30 min) in the absence of any catalyst. The detailed results are shown in Fig. 1(c). The effect of the solid–liquid ratio on the formation of HC differed from that of reaction temperature/time. An increase in the solid–liquid ratio caused the yield of HC to increase gradually from 65.67 wt% (0.03 g/mL) to 74.92 wt% (0.25 g/mL). Cao et al. (2019) also found that an increase in biomass loading from 5% to 10% promoted the yield of HC by 5.2% during the microwave-assisted HTC of *Gracilaria lemaneiformis*. As shown in Fig. 1(c), the content of VOM in HC gradually increased with the increasing solid–liquid ratio. In other words, the conversion efficiency of SS decreased with an increase in the solid–liquid ratio. This result occurred primarily because the penetration depth of microwave energy is limited. With an increase in the solid–liquid ratio, more mass barriers must be overcome by microwaves, reducing the degradation efficiency of the biomass polymerization structure (Kang et al., 2019). In addition, increasing the solid–liquid ratio suggests a higher mass transfer resistance and lower substrate accessibility with water molecules. Although the O/C atomic ratio of HC gradually decreased with an increase in the solid–liquid ratio, indicating an increase in the carbonization degree of HC, the H/C atomic ratio of HC continuously increased (that is, the aromatization degree of HC decreased), indicating that the stability of HC in soil would decrease (Fig. 1(c)). Generally, a lower solid–liquid ratio facilitated the faster conversion of organics in SS resulting in a low yield of HC and a low content of VOM. With an increase in the solid–liquid ratio, the concentration of monomers in the liquid phase quickly increased, which promoted the polymerization to start earlier, leading to an increase in the HC yield (Wang et al., 2019a; Wang et al., 2020c).

3.4. Influence of catalyst

Microwave-assisted HTC of SS with two catalysts, H_3PO_4 and CaO, was conducted at 230 °C with a fixed reaction time (30 min) and solid–liquid ratio (0.03 g/mL). The effects of the addition of catalysts on the formation of HC are shown in Fig. 2. The use of H_3PO_4 as a catalyst reduced the yield of HC from 65.67 wt% (no catalyst) to 59.31 wt% (0.6 mol/L H_3PO_4) (Fig. 2(a)). In other words, the addition of phosphoric acid promoted the degradation and transformation of SS to a certain extent, as evidenced by the decrease in VOM in HC and the significant increase in EC in PW (2.18 ms/cm [no catalyst] to 9.83 ms/cm [0.6 mol/L H_3PO_4]). A similar phenomenon has been reported in the microwave-assisted HTC of *Chlorella vulgaris* (ESP-31) with H_3PO_4 (0–0.1 mol/L) used as a catalyst (Gan et al., 2020). In general, the acid catalyst would enhance the hydrolysis reaction in the HTC of biomass, and the conversion of biomass was correspondingly improved, resulting in a decrease in HC yield (Nizamuddin et al., 2017).

In contrast, the application of CaO as a catalyst increased the yield of HC from 65.67 wt% (no catalyst) to 80.31 wt% (10% CaO) (Fig. 2(b)). The specific reason for this result was that the addition of CaO enhanced the formation of calcium carbonate during the HTC process (Lang et al., 2019b). This finding was consistent with the results of the study by Wang et al. (2020a); the addition of CaO also promoted the formation of HC during the microwave-assisted HTC of swine manure. Notably, the addition of H_3PO_4 caused the pH values of HC and PW to decrease, indicating strong acidity with a high dosage of H_3PO_4 , while the addition of CaO increased the pH value of HC and PW that indicated alkalinity (Table S2). Based on this finding, it was realized that the products obtained by using CaO as a catalyst may be easier to be applied (e.g., land use of HC) or further treatment (for example, anaerobic digestion of PW) than those produced with H_3PO_4 as a catalyst.

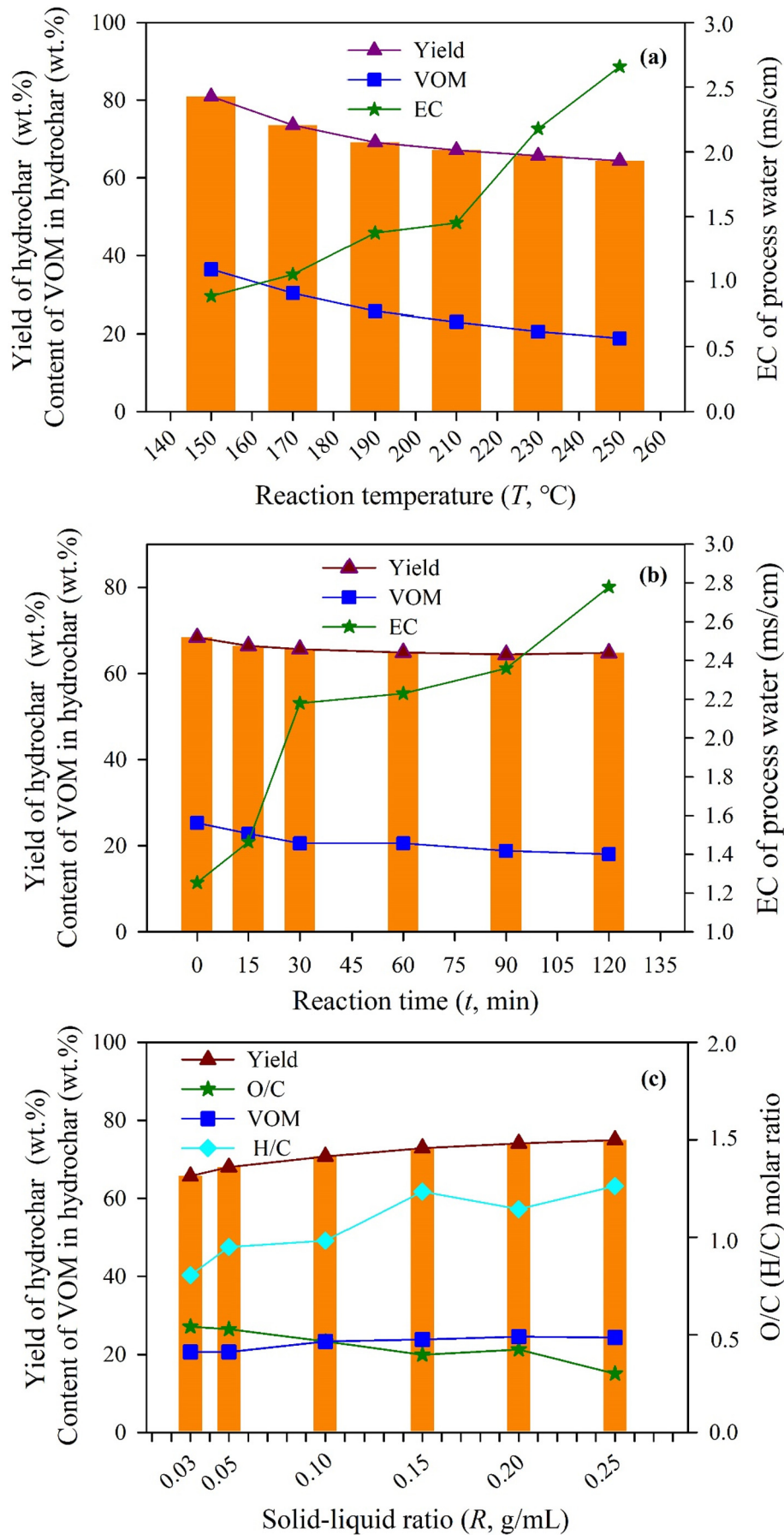


Fig. 1. Effects of reaction temperature (T , a), reaction time (t , b), and solid-liquid ratio (R , c) on the microwave-assisted HTC of SS.

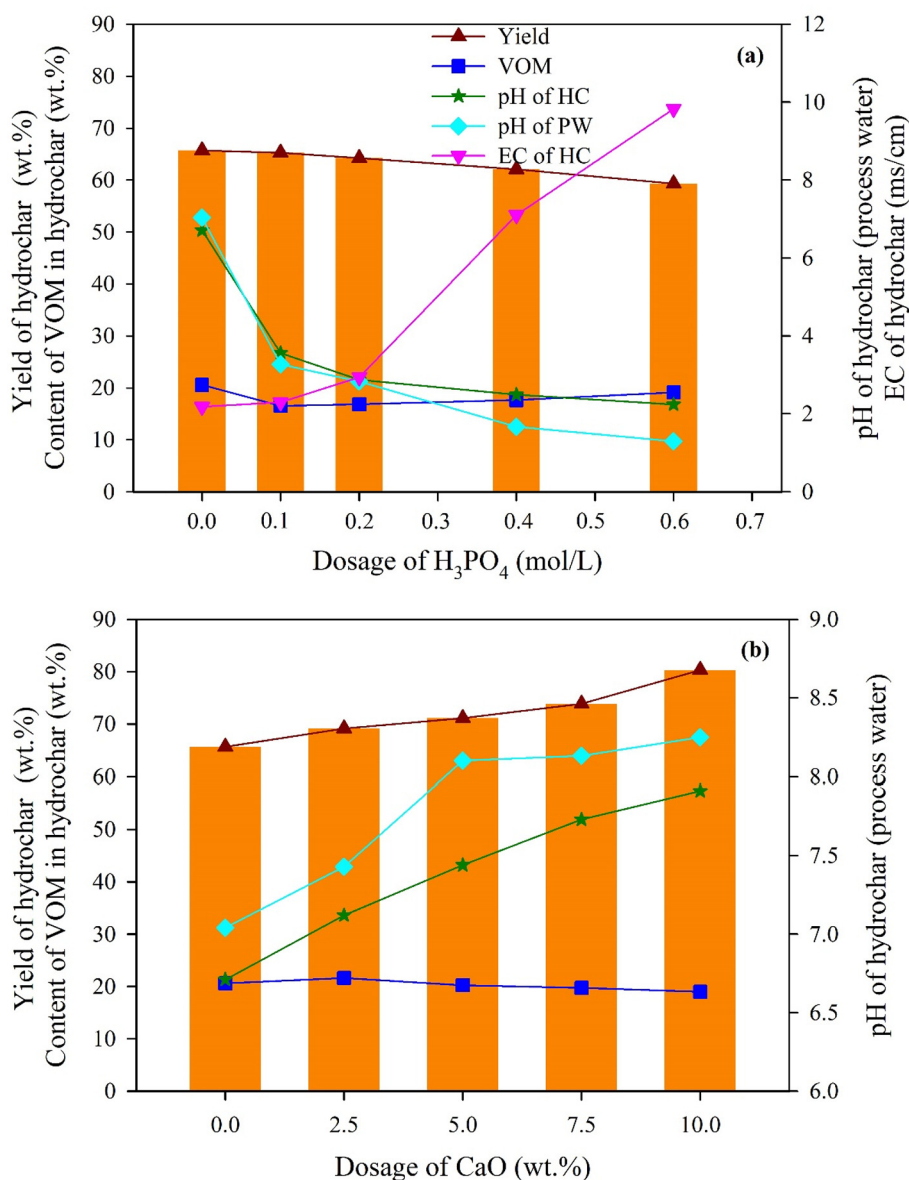


Fig. 2. Effects of catalysts on the microwave-assisted HTC of SS, (a) H₃PO₄, (b) CaO.

3.5. Characteristics of HC

In the following sections, the main characteristics of representative HTC products (HC and PW [discussed in Section 3.6]) are systematically described. The reaction temperature and reaction time were fixed at 230 °C and 30 min, respectively, mainly considering the pH value of PW. As shown in Tables S3 and S4, if the reaction temperature is

lower than 230 °C or the reaction time is less than 30 min, the PW is acidic, which is not conducive to its treatment or utilization. The higher reaction temperature and reaction time mean greater energy consumption. In addition, the selection of the solid-liquid ratio of 0.03 g/L mainly considered the H/C atomic ratio of HC. As shown in Table S5, the higher the solid-liquid ratio, the higher the H/C ratio of HC, which means the lower aromaticity of HC, resulting in lower stability of HC in the soil.

Table 1
CV, elemental and proximate analysis of SS and HCs.

Items	Proximate analysis (wt%) ^a			Elemental analysis (wt%) ^a				Atomic ratio			C/N ratio	CV (MJ/kg)
	VOM	FC	Ash	C	H	O ^b	N	O/C	H/C	(N + O)/C		
SS	43.81	2.65	53.54	21.76	3.44	17.58	3.69	0.61	1.90	0.48	5.90	9.52
HC ^c	20.56	2.52	76.92	12.37	0.83	8.94	0.95	0.54	0.81	0.59	13.02	4.52
HC-CaO (5.0 wt%) ^c	20.22	1.12	78.30	11.70	0.68	8.47	0.87	0.54	0.69	0.61	13.52	4.17
HC-H ₃ PO ₄ (0.2 mol/L) ^c	16.84	1.48	82.04	11.09	<0.3	6.22	0.65	0.42	<0.32	0.47	17.05	3.57

^a On a dry basis.

^b O% = 100% - Ash% - C% - H% - N%.

^c All HCs were obtained at 230 °C for 30 min with a solid-liquid ratio of 0.03 g/mL.

3.5.1. General characteristics

The elemental/proximate compositions of raw SS and representative HCs are listed in Table 1. The SS feedstock was different from other biomass (e.g., lignocellulose, algae); the ash content of SS was very high, and accordingly, its calorific value was relatively low (Fonts et al., 2012). For example, the ash content in the raw SS tested in this study was as high as 53.54 wt%, and its calorific value was only 9.52 MJ/kg. The dissolution and degradation of organic matter contained in SS during the microwave-assisted HTC process led to a decrease in the VOM content in the HCs. However, the mineral components were generally retained in HCs due to the precipitation of minerals in ash and deposition of some inorganic substances on HC, and thus, increasing the content of ash (Gao et al., 2018; Tasca et al., 2019). Hence, the caloric values of HCs were lowered to 3.57–4.52 MJ/kg. The addition of catalysts, especially H_3PO_4 , further decreased the content of organic matter in the HC while increasing the content of ash. The addition of catalysts is posited to promote the degradation of organic compounds and the formation of some inorganic metal salt precipitates (see Fig. S1 in the Supplemental material) (Lang et al., 2019b).

HCs, especially for those produced in the catalytic HTC runs, contained lower contents of C, H, O, and N than raw SS feedstock, and thus possessed a higher $(N + O)/C$ molar ratio and lower O/C and H/C molar ratios (Table 1). The decrease in the nitrogen content of HC may be primarily ascribed to the solubilization or degradation of proteinaceous components (Hämäläinen et al., 2021; Malhotra and Garg, 2020). According to the Van Krevelen diagram for raw SS and its HC (Fig. 3), it was inferred that the decarboxylation and dehydration reactions were the two main formation pathways of HCs, resulting in a decrease in the contents of C, H and O. Furthermore, the dehydration reaction (formation of water) was more important than the decarboxylation reaction (formation of carbonyls, carboxylic acids, and CO_2), now that the H/C molar ratio showed a greater decrease than the O/C molar ratio (Zhang et al., 2021b). The $(N + O)/C$, O/C , and H/C molar ratios are usually considered as indicators of polarity, carbonization degree, and aromaticity of HC, respectively. Lower the O/C and H/C molar ratios, higher the aromaticity and carbonization degree. Lower the $(N + O)/C$ molar ratios, lower the polarity (Wang et al., 2020b). Thus, the HCs had higher aromaticity and carbonization degree than

Table 2
pH, EC, and major nutrients of SS and HCs.

Items	pH	EC (mS/cm)	Nutrients (g/kg)				
			TP ^a	TK ^a	SP ^b	SK ^b	SN ^b
SS	6.03	1.47	13.50	5.00	0.85	2.55	3.88
HC ^c	5.97	0.37	20.97	3.70	0.32	0.43	0.79
HC-CaO (5.0 wt%) ^c	7.44	0.43	21.89	6.60	0.04	4.04	0.55
HC- H_3PO_4 (0.2 mol/L) ^c	2.87	1.43	100.01	4.31	2.40	3.54	0.83

^a Indicates total content.

^b Indicates available content.

^c All HCs were obtained at 230 °C for 30 min with a solid-liquid ratio of 0.03 g/mL.

the raw SS feedstock, and their polarity increased (except for the HC generated in the H_3PO_4 -catalytic run).

After the HTC treatment, the C/N ratio was increased from 5.90 (SS) to 13.03–17.05 (HCs). Higher is the C/N ratio, lower is the availability of N. In other words, the HTC treatment process exhibited an immobilization effect on N, which was confirmed by the decrement of soluble N in HCs (0.55–0.83 g/kg versus 3.88 g/kg; Table 2). In addition, if the HC product is applied for agricultural use, the C/N ratio of HC should not exceed 20; otherwise, sufficient available nitrogen will not be assured for crop utilization (Wang et al., 2020a). Fortunately, the C/N ratios of all HCs in this study were below the specified values.

Table 2 shows the pH, EC, and major nutrients of raw SS and the selected HCs. The raw SS feedstock was weakly acidic, with a pH value of 6.03. Compared with raw SS, the HC possessed a slightly lower pH value (HC, 5.97) because of the residual of partial organic acids formed during the HTC process (Xiong et al., 2019). The addition of H_3PO_4 further reduced the pH of HC to 2.87 (HC- H_3PO_4), whereas the addition of CaO improved the pH of HC to 7.44 (HC-CaO). The acidity and basicity of the catalyst may be an important reason for the change in the pH value of HC. The HTC process often has a certain desalination effect (Jin et al., 2019). Thus, it was found that the EC value of HC (0.37 mS/cm) was lower than that of raw SS (1.47 mS/cm). Notably, the addition of catalysts promoted the EC of HC, especially for HC- H_3PO_4 with an EC value of 1.43 mS/cm.

The contents of TP and TK in raw SS were 13.50 g/kg and 5.00 g/kg, respectively. Phosphorus was further enriched in the HC (20.97 g/kg)

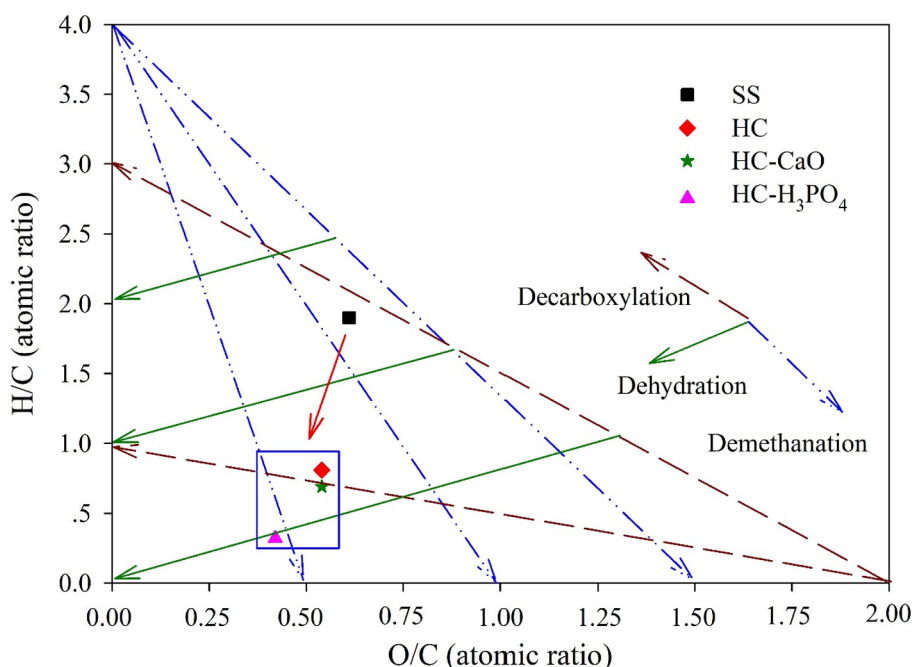


Fig. 3. Van Krevelen diagram for raw SS and HCs obtained at 230 °C for 30 min with a solid-liquid ratio of 0.03 g/mL.

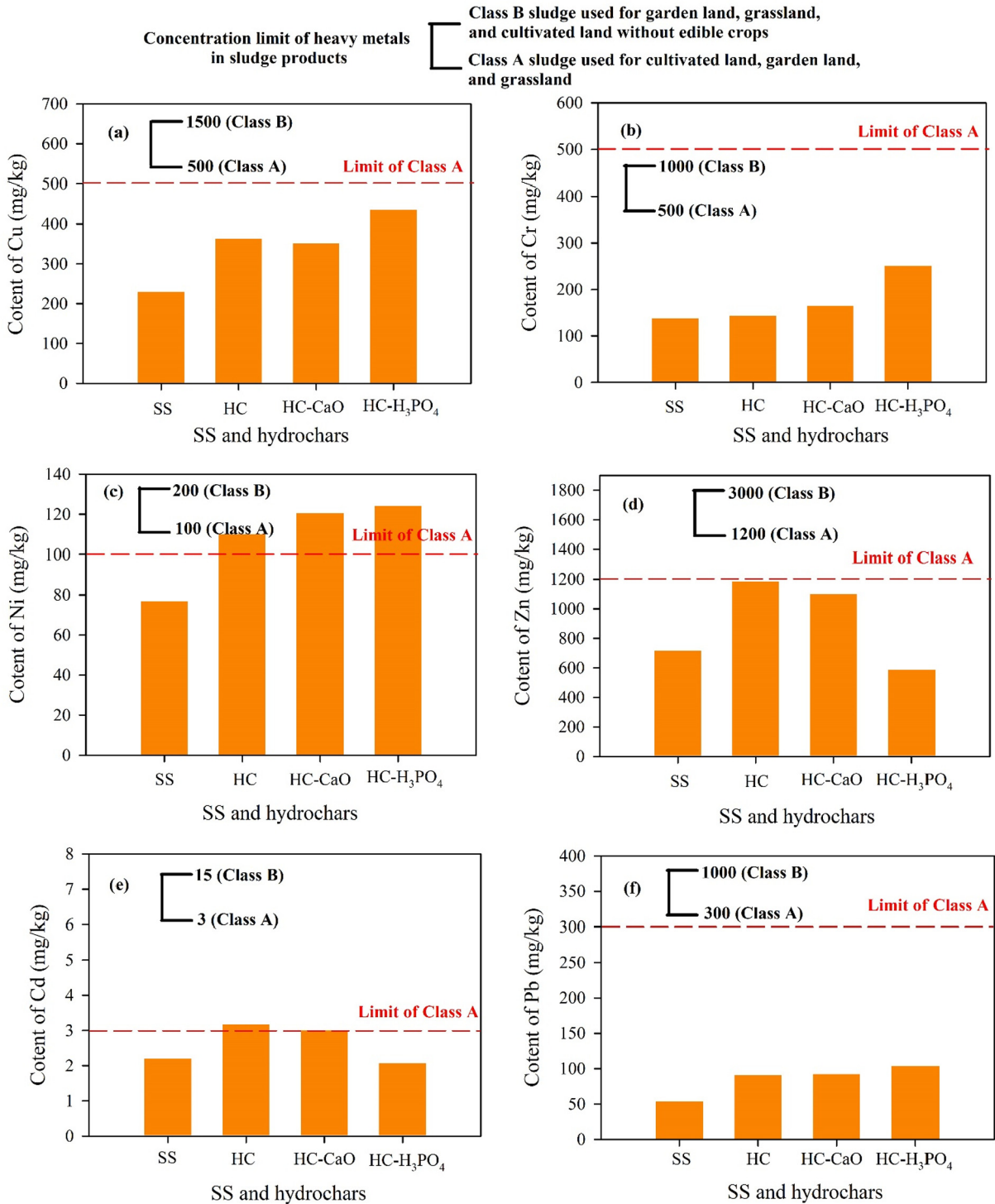


Fig. 4. Total content of heavy metals in raw SS and HCs obtained at 230 °C for 30 min with a solid-liquid ratio of 0.03 g/mL.

after the HTC treatment because of the formation of precipitated phosphate salts, and the potassium content was reduced to 3.70 g/kg, which usually possessed a high affinity with PW (Hämäläinen et al., 2021; Heilmann et al., 2014). The changes in the content of SP and SK were consistent, and decreased from 0.85 g/kg to 0.32 g/kg and from 2.55 g/kg to 0.43 g/kg, respectively. The use of CaO as the catalyst slightly increased the TP content in the HC, and the content of SP was further reduced to 0.04 g/kg. Notably, the content of TK in HC increased to 6.60 g/kg, which was even higher than that in raw SS, resulting in an increase

in SK to 4.04 g/kg. A study by Deng et al. (2020) proved that calcium ions can react with P to form insoluble phosphates (hydroxyapatite and octa-calcium phosphate). In the case of using H₃PO₄ as the catalyst, the TP content in HC was significantly increased, up to 100.01 g/kg, and the corresponding SP content was also improved to 2.40 g/kg. This may be attributed to the addition of a large amount of phosphorus into the reaction system by the phosphoric acid catalyst itself. The effect of the H₃PO₄ catalyst on the total potassium and soluble potassium content in HC was similar to that of the CaO catalyst.

3.5.2. Heavy metals content

The identification of the occurrence characteristics of heavy metals in HC is helpful for judging the control effect of the microwave-assisted HTC process on heavy metal pollution. The total contents of heavy metals in raw SS and HCs are shown in Fig. 4. In Fig. 4, the specified values of heavy metals in a national standard are also quoted, which focuses on the control standards of pollutants in sludge for agricultural use (Table S6). In the raw SS feedstock, Zn possessed the highest concentration (717.02 mg/kg), followed by Cu (229.64 mg/kg), Cr (136.85 mg/kg), Ni (76.78 mg/kg), Pb (53.79 mg/kg), and Cd (2.20 mg/kg). Notably, the contents of the six heavy metals were all under the prescribed values of Class A (Table S6), indicating that the corresponding SS can be applied to arable land, garden land, and grassland. Compared with raw SS, the HC contained a higher total content of heavy metals, especially for Zn and Cu, increasing by 468.78 mg/kg and 132.88 mg/kg, respectively. In addition, the contents of Cd and Ni in HC exceeded the prescribed values of Class A but were still under those of Class B, indicating that the HC product cannot be applied to edible crops in arable land. The enrichment of heavy metals in HC can be ascribed to the heavy metals being very stable under a relatively mild treatment process (150–250 °C in this study) rather than being converted or volatilized (Wang et al., 2019a). In addition, the degradation/transformation of organic matter in SS during the HTC process indirectly increased the total content of heavy metals (Hämäläinen et al., 2021; Huang and Yuan, 2016). Some heavy metals (for example, Zn and Cu) might form precipitations due to their low water solubility and cation exchange capacity under HTC conditions (Lu et al., 2021).

When CaO was introduced during the microwave-assisted HTC of SS, the total contents of Cu, Cd, and Zn in HC (HC–CaO) were reduced, which can be ascribed to the increase in HC yield. However, a slight increase was observed in the total contents of Cr, Ni, and Pb. This may be because of the addition of CaO, which inhibited the dissolution of the metals in the reaction process and reduced their transfer to PW. In the presence of H₃PO₄, the total contents of Cu, Cr, Ni, and Pb in HC (HC–H₃PO₄) were further increased to different extents. There are two reasons for the above results. First, the yield of HC decreased when H₃PO₄ was used as a catalyst, which indirectly increased the total content of heavy metals in the HC. Second, the phosphoric acid compounds of the above metals were insoluble in water. As for the decrease in Cd and Zn contents, it was speculated that Cd and Zn were easily transferred to PW under acidic reaction conditions. However, the addition of catalysts did not improve the agricultural utilization of HC; moreover, the HC produced could not be used for the cultivation of edible crops. This problem can be solved by introducing other biomass with low content of heavy metals in the microwave-assisted HTC of SS (also known as co-HTC treatment) (Shi et al., 2013).

The leachability of the heavy metals was also evaluated by analyzing their leachable contents (Table 3). The leachable contents of all six heavy metals in HC were lower than those in raw SS. This was mainly because the HTC process had a certain passivation effect on the heavy metals in the SS. Specifically, HTC treatment decreased the directly bioavailable and potentially bioavailable fractions of heavy metals decreased, and the residual fraction showed an observable increase

(Wang et al., 2019b; Zhang et al., 2018). Notably, the introduction of CaO further reduced the leaching capacity of heavy metals in the HC, whereas H₃PO₄ had the opposite effect. The leachable contents of Zn, Pb, and Cd in HC (HC–H₃PO₄) were even higher than those in raw SS, but still lower than the threshold for hazardous waste (Table S7). These results may be associated with the changes in the pH values of the HC (Table 2).

3.5.3. Combustion characteristics

Fig. 5 presents the TG–DTG curves of raw SS feedstock and HCs obtained at 230 °C with or without catalysts, revealing that the SS-derived HC possessed distinct combustion behavior compared with the raw SS feedstock. Furthermore, the addition of catalysts during the HTC process further changed the combustion behavior of HCs. According to Fig. 5(a), the SS combustion process comprises of three stages. Stage A ranged from 30 °C to 120 °C, mainly due to the initial water evaporation. In stage B (150–400 °C), the combustion of the partial volatile matter was the main loss. Stage C ranged from 400 °C to 550 °C, mainly attributed to the oxidation of residual volatile matter and FC. After this stage, it was mainly the degradation of inorganic substances (Peng et al., 2016). Regarding HCs, a similar stage A was observed, with a lower peak DTG value than that of the raw SS feedstock, which was probably because of the higher percentage of bound water in the original SS (Zhang et al., 2021a). In the second stage (stage B), the maximum weight loss rate values (DTG_{max}) were all lowered, and the corresponding peak temperatures (T_m) were delayed because of the decrease in volatile matters in the HCs. The peak temperature of stage C in HC obtained in the non-catalytic run declined to approximately 400 °C (Fig. 5(b)). When H₃PO₄ was used as the catalyst, the peak temperature of stage C increased to 500 °C (Fig. 5(c)). When CaO was applied as the catalyst, stage C was unapparent and was accomplished all with stage B (Fig. 5(d)).

Table 4 displays the characteristic combustion parameters of raw SS and representative HCs. The T_i was increased from 215.46 (raw SS) to 241.54 °C (HC), and the T_b was decreased from 517.45 to 463.66 °C. The application of CaO as a catalyst further improved the T_i to 261.87 °C and slightly reduced the decline range of T_b . Notably, the T_i of HC was also further improved to 331.21 °C with the addition of H₃PO₄, but at the same time, the T_b of hydrochar also was increased from 517.45 to 536.34 °C. The increase in T_i and the decrease in T_b of HC were mainly due to the degradation/transformation of organic matter in the HTC process, resulting in a decrease of residual organic matter content in the HCs (Table 1) (Lu et al., 2021). The addition of catalysts further promoted the degradation of organic matter, and thus, T_i was further increased. A high T_i indicates a lower fire and explosion risk; this means that there was a higher security in the treatment, storage, and transportation of HC than raw SS (Peng et al., 2016). Special attention should be paid to the increase in the T_b of HC, especially when H₃PO₄ was used as the catalyst (even higher than that of the raw SS). This may be because the application of the catalyst promoted the formation of aromatic compounds with a stable structure in HC (please refer to the H/C molar ratio listed in Table 1) (Lang et al., 2019a).

The increase in R_m from 51.87 wt% in raw SS to 75.94–81.98 wt% in HCs is possibly because of the accumulation of ash in HCs. Significantly, the values of R_m were all slightly lower than the corresponding ash content (Table 1), indicating that the combustion process of raw SS materials and HCs was relatively thorough. The DTG_{max} , CCI , and CSI values of the HCs were lower than those of the raw SS feedstock. Similar results were reported by He et al. (2013), who carried out the conventional HTC of SS at 200 °C for 4–12 h. The lower values of DTG_{max} , CCI , and CSI in HCs may be because the HTC treatment resulted in a substantial loss of organic matter in the HCs. In contrast, a high content of organic matter would also lead to flame instability, resulting in high heat loss. Overall, the combustion performance of SS was considered to be poor, although it presented high CCI and CSI values (Wang et al., 2020c). Notably, the addition of H₃PO₄ significantly further reduced the DTG_{max} , CCI , and

Table 3

Contents of leachable heavy metals in raw SS and HCs (mg/L).

Items	Cu	Zn	Pb	Cr	Cd	Ni
SS	2.33	1.16	0.03	0.21	0.004	2.20
HC ^b	0.18	0.50	0.01	0.09	– ^a	0.08
HC–CaO (5.0 wt%) ^b	0.12	0.53	0.01	0.06	–	0.03
HC–H ₃ PO ₄ (0.2 mol/L) ^b	1.75	4.55	0.19	0.07	0.008	0.09
Standard value ^c	100	100	5.0	15.0	1.0	5.0

^a Under the detect limit.

^b All hydrochars were obtained at 230 °C for 30 min with a solid–liquid ratio of 0.03 g/mL.

^c Identification standards for hazardous wastes (Table S7).

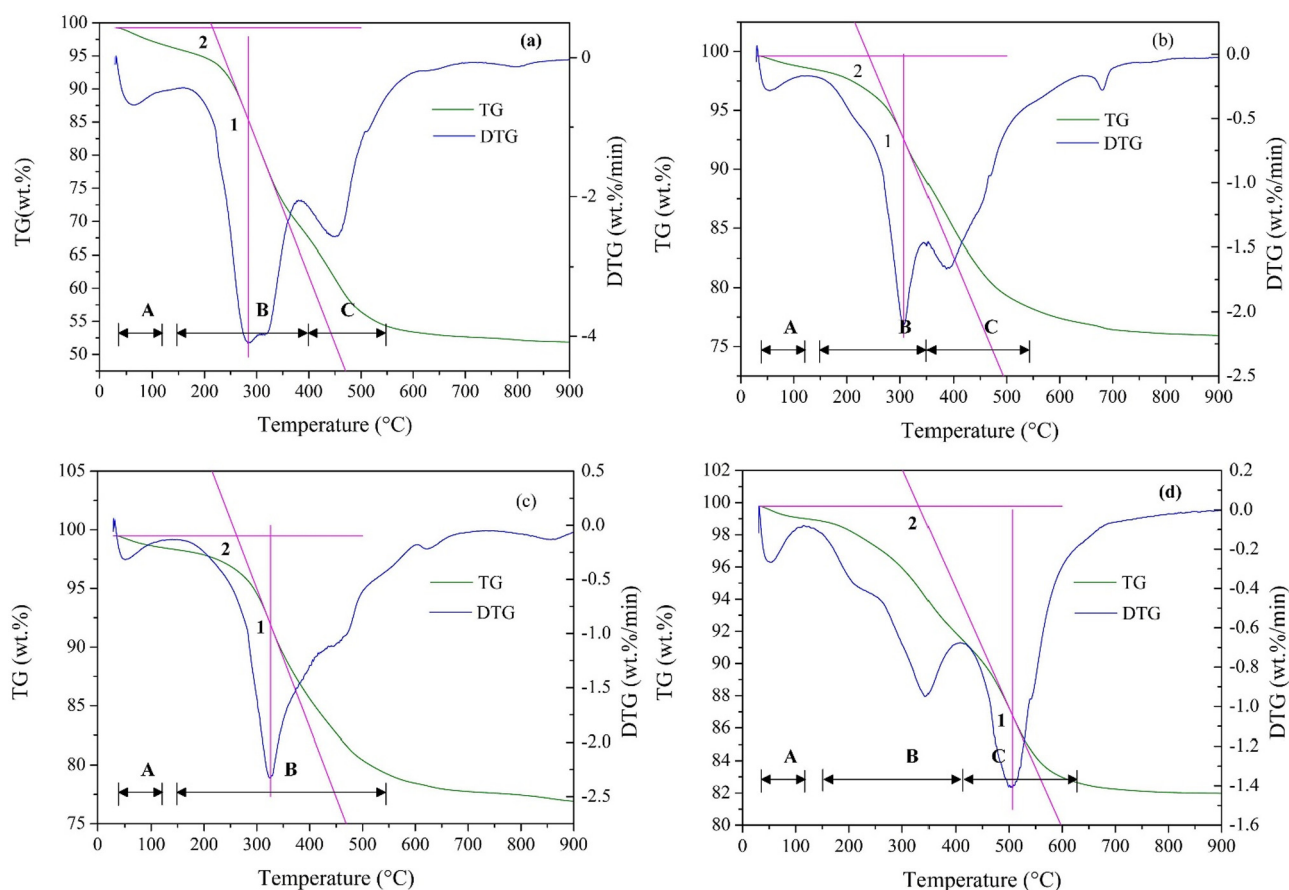


Fig. 5. TG-DTG curves of raw SS (a) and HCs ((b) HC, (c) HC-CaO, and (d) HC-H₃PO₄) obtained at 230 °C for 30 min with a solid-liquid ratio of 0.03 g/mL.

CSI values of HC. He et al. (2019), Lu et al. (2021) and Wilk et al. (2021) improved the combustion performance of SS-derived hydrochar by introducing sawdust, charcoal, polyvinyl chloride, walnut shell, fallen leaves and orange peel in the conventional HTC process. The introduction of similar biomass into microwave-assisted HTC of SS is also expected to improve the combustion performance of hydrochar, which needs further research.

3.5.4. Micromorphology and surface characteristics

Fig. 6 presents the N₂ adsorption/desorption isotherms and pore size distributions of the HCs. Specific surface areas, pore sizes, and pore volumes of the HCs are listed in Table 5. According to the pore size, the pores are usually classified as micropores (<2 nm), mesopores (2–50 nm), and macropores (>50 nm) (Lai et al., 2018; Pan et al., 2018). The average pore size of hydrochars was ranked in the range of

10.1–22.6 nm (Table 5), indicating that the SS-derived HCs produced in this study were mesoporous materials. All three HCs exhibited a Type IV sorption isotherm with a typical hysteresis loop (Fig. 6(a, c, e)), characteristic of mesoporous and nonporous adsorbents. The hysteresis loops were a Type H3 loop, usually observed with aggregates of plate-like particles giving rise to slit-shaped pores (Sing et al., 1985).

The pore size distribution of HCs presented a similar peak horizontal position (about 1.0 nm) (Fig. 6(b, d, f)). Some differences among the three types of HCs were also observed. The percentages of micropores, mesopores, and macropores in HC derived from the non-catalytic run were 0.60%, 49.52%, and 49.89%, respectively (Table 5). The use of CaO as a catalyst improved the proportions of micropores and mesopores, and in the case of H₃PO₄, the number of mesopores was decreased and the number of micropores and macropores increased. Thus, the average pore size of HC was significantly reduced from 22.6 nm (HC) to 10.1 nm (HC-CaO), and for HC-H₃PO₄, only a slight decrement was observed. The addition of both catalysts reduced the pore volume and specific surface area of the HC. Based on this, it was inferred that the degradation of SS components was enhanced by the application of catalysts (Table 1); and thus, more small plate-like particles were formed, which may block or squeeze part of the pores (Fig. 6). During the microwave-assisted HTC of crop residues, it was found that the application of H₃PO₄ could improve the pore volume and specific surface area of HC (Liu et al., 2021c). The main reason for this conflict may be the different compositions and structures of SS and crop residues.

The changes in the micromorphology of SS before and after HTC treatment are shown in Fig. 7. The raw SS feedstock presented a flat, smooth, and dense matrix (Fig. 7(a)). After the HTC treatment, the surface of the HC became coarser/disoriented and contained more pores, indicating the disintegration of the SS matrix. Additionally, some

Table 4
Characteristic combustion parameters of raw SS and HCs.

Items	SS	HC ^a	HC-CaO (5.0 wt%) ^a	HC-H ₃ PO ₄ (0.2 mol/L) ^a
T _i (°C)	215.46	241.54	261.87	331.21
T _b (°C)	517.45	463.66	471.19	536.34
T _m	283.88	306.97	325.82	506.28
DTG _{max} (wt%/min)	4.11	2.10	2.33	1.41
DTG _{mean} (wt%/min)	1.07	0.54	0.51	0.40
R _m (wt%)	51.87	75.94	76.92	81.98
CCI (10 ⁻⁸ , wt% ² min ⁻² °C ⁻³)	18.31	4.19	3.68	0.96
CSI (10 ³ , wt%min ⁻¹ °C ⁻²)	5.77	2.43	2.35	0.72

^a All HCs were obtained at 230 °C for 30 min with a solid-liquid ratio of 0.03 g/mL.

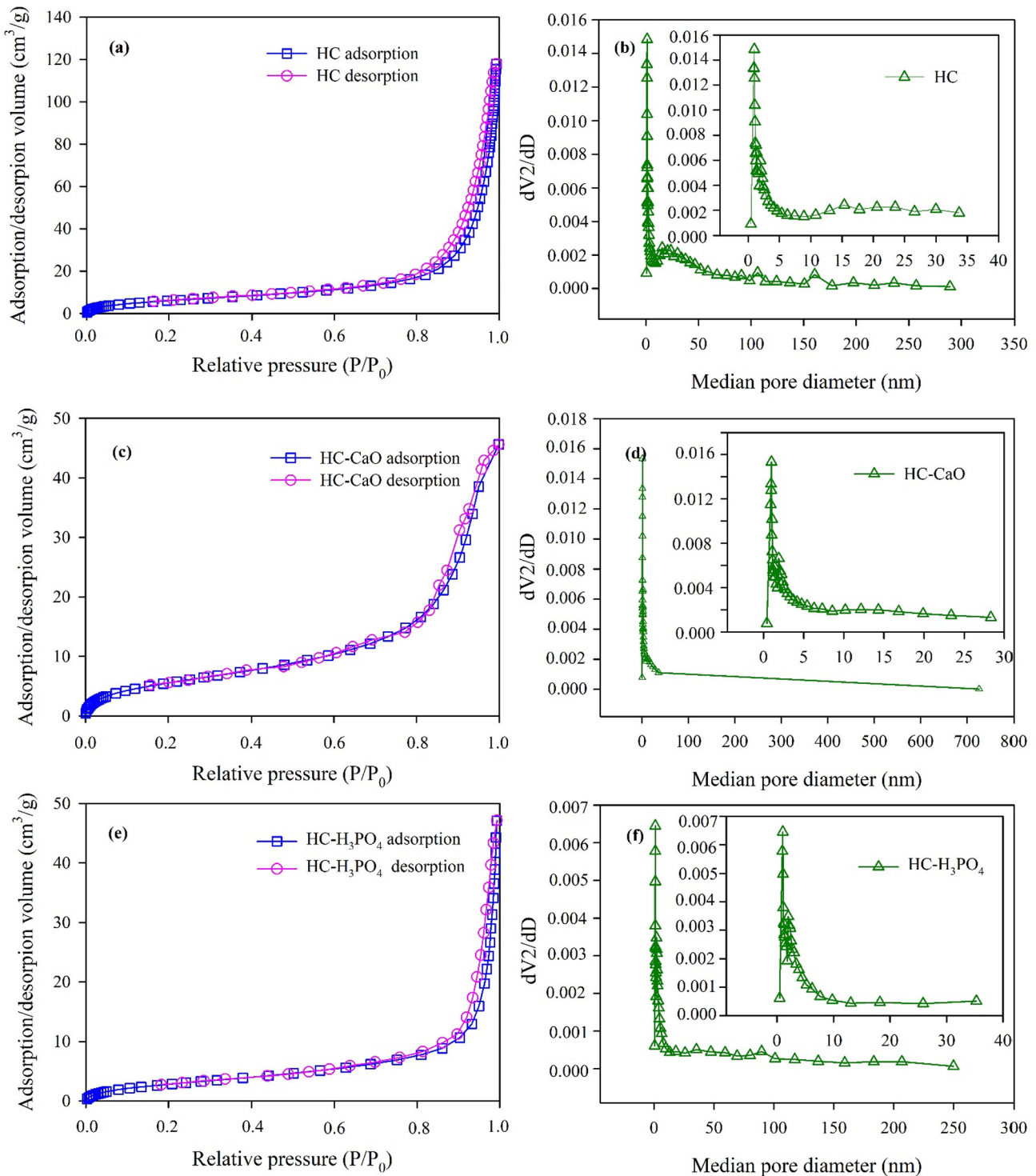


Fig. 6. N_2 adsorption-desorption isotherms and pore size distribution of HCs obtained at 230 °C for 30 min with a solid-liquid ratio of 0.03 g/mL. HC: (a) and (b); HC-CaO: (c) and (d); HC- H_3PO_4 : (e) and (f).

crystalline substances were present on the surface of the HC (Fig. 7(b)). The morphology of HC was related to the transformation and volatilization of organic matter in the feedstock (He et al., 2013; Wang et al., 2021). The addition of catalysts, especially H_3PO_4 , enhanced the decomposition of organic matter in SS, as shown in Table 1. Thus, the surface of HC-CaO presented flocculent structures comprising smaller particles (Fig. 7(c)), and a honeycomb structure formed by debris accumulation was observed on the surface of HC- H_3PO_4 (Fig. 7(d)).

3.6. Characteristics of PW

Table 6 shows the major properties of the representative PW produced from the microwave-assisted HTC of SS. When no catalyst was used, the pH value of the PW was 7.04, indicating neutral properties. Normally, the hydrolysates of SS components (various organic acids) generated during HTC would lead to the acidic properties of the PW (Liu et al., 2021c). However, the final pH of the PW was also affected

Table 5
Specific surface area, pore size, and pore volume of HCs.

Items	HC ^a	HC-CaO (5.0 wt%) ^a	HC-H ₃ PO ₄ (0.2 mol/L) ^a
Specific surface area (m ² /g) ^b	24.0	21.8	11.4
Average pore size (nm) ^c	22.6	10.1	19.8
Micropore volume (cm ³ /g) ^c	0.0079	0.0071	0.0037
Pore volume (cm ³ /g) ^c	0.189	0.076	0.076
Pore size distribution (%) ^d	≤2.0 nm	0.60	1.98
	3–10 nm	9.32	28.45
	11–50 nm	40.20	57.48
	51–100 nm	21.09	0.89
	101–200 nm	19.52	1.79
>200 nm	9.28	9.41	7.68

^a All HCs were obtained at 230 °C for 30 min with a solid–liquid ratio of 0.03 g/mL.

^b BET (Brunauer–Emmett–Teller) multipoint method.

^c HK (Horvath and Kawazoe) method (pore size range: <2 nm).

^d BJH (Barrett–Joyner–Halenda) method, adsorption data (pore size range: 1.7–300 nm).

by volatilization, for example, of ammonia, during the HTC treatment (Hämäläinen et al., 2021). Wilk et al. (2019) performed the conventional HTC of SS at 200 °C for 4 h and found a similar result that the pH of PW was 7.33. It was predictable that the application of CaO as a catalyst made the pH of PW increase to 8.10 (alkaline properties), and the use of H₃PO₄ as a catalyst made the pH of PW reduce to 2.83 (strong acidity). The EC value of PW was increased from 2.18 ms/cm (PW, without catalyst) to 2.25 ms/cm (PW–CaO) and 2.94 ms/cm (PW–H₃PO₄), respectively. The presence of H₃PO₄ might enhance the dissociation of base ions in the raw SS, resulting in many solutes entering the PW,

Table 6
Major characteristics of PW (mg/L).

Items	pH	EC (ms/cm)	SP	SK	NH ₄ ⁺ -N	COD
PW ^a	7.04	2.18	36.22	0.06	502.40	1366.88
PW–CaO (5.0 wt%) ^a	8.10	2.25	4.69	0.07	478.35	2526.98
PW–H ₃ PO ₄ (0.2 mol/L) ^a	2.83	2.94	6566.70	0.11	782.19	1714.38

^a All PW were obtained at 230 °C for 30 min with a solid–liquid ratio of 0.03 g/mL.

and thus increasing the EC value of PW (Xiong et al., 2019). The addition of CaO during the HTC process reduced the contents of SP and NH₄⁺-N in the PW, and an opposite trend was observed for H₃PO₄. The specific reason for this result may be that the application of H₃PO₄ promoted the deamination reactions of proteinaceous compounds and introduced available phosphorus components. The addition of CaO might enhance the formation of apatite inorganic phosphorus (phosphate bound to Ca) (Zhang et al., 2017). The COD value of PW was increased from 1366.88 mg/L (PW) to 2526.98 mg/L (PW–CaO) and 1714.38 mg/L (PW–H₃PO₄), respectively, suggesting that the addition of catalyst enhanced the degradation of organic matters in raw SS. At present, the further recovery of energy, nutrients and chemicals from process water is becoming one of the hot spots of researchers (Leng et al., 2020; Leng et al., 2021; Usman et al., 2019).

3.7. Formation pathways and potential application of HCs

Based on the literature review and the findings of this study, the formation pathways of HC during the microwave-assisted HTC of SS were preliminarily conjectured (He et al., 2013; Liu et al., 2021a;

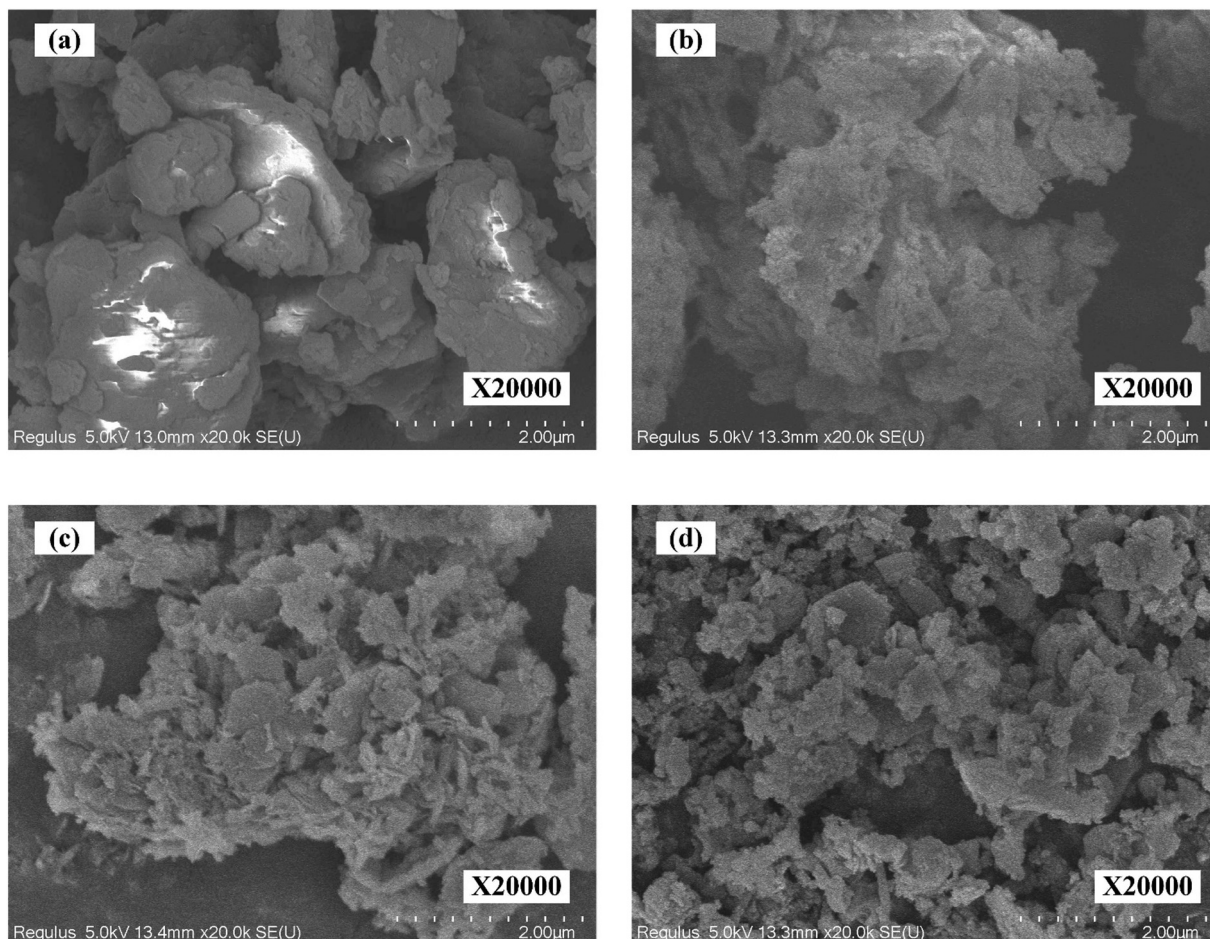


Fig. 7. SEM analysis of raw SS (a) and HCs ((b) HC, (c) HC–CaO, and (d) HC–H₃PO₄) obtained at 230 °C for 30 min with a solid–liquid ratio of 0.03 g/mL.

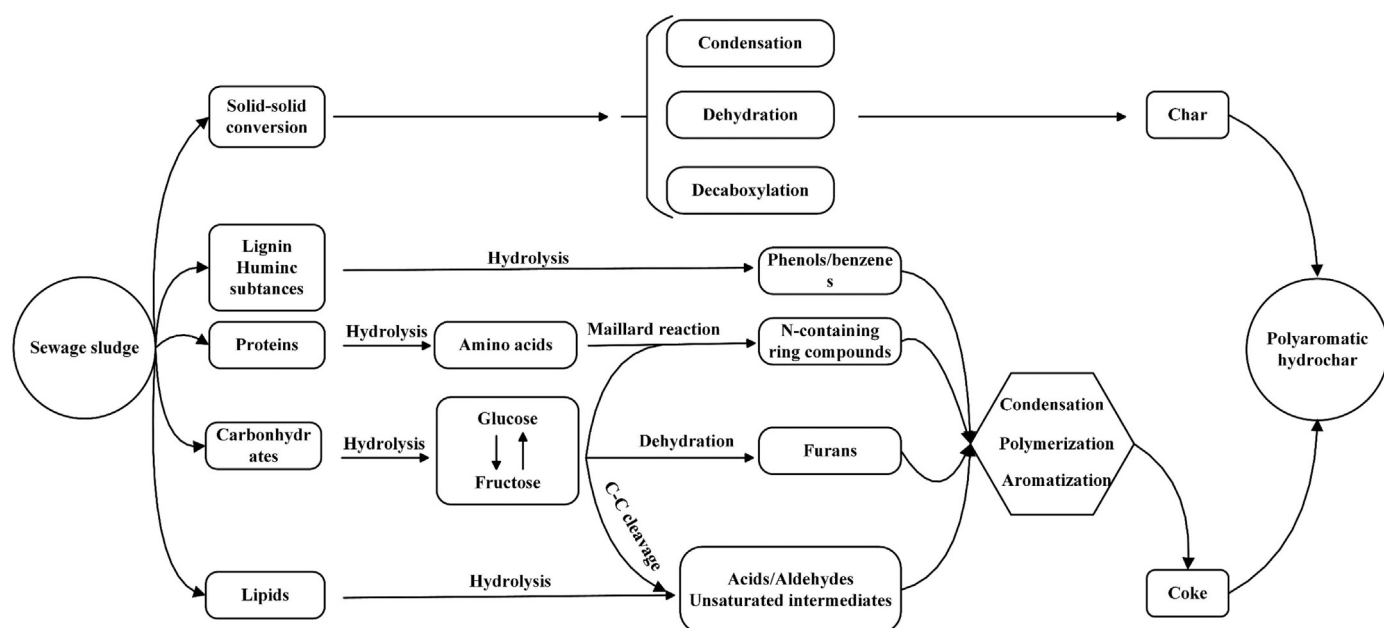


Fig. 8. Speculated formation mechanism of HC (Summarized from references: He et al., 2013; Liu et al., 2021a; Wang et al., 2019a).

Wang et al., 2019a). As shown in Fig. 8, the HC can be formed through two main reaction pathways: direct solid-solid conversion, also known as 'char', and aggregation of degradation intermediates from the organic components (lipids, carbohydrates, proteins, lignin, and humic substances), also known as 'coke'. The actual HC production process is much more complex than that shown in Fig. 8. Special experiments must be designed to determine the detailed formation mechanism of HC in the microwave-assisted HTC of SS (Yu et al., 2020b). Although HCs have shown great potential to be used in materials, energy, agriculture, and environment, the high ash content in SS-derived HCs may limit their application potential to a certain extent (Liu et al., 2021d; Wang et al., 2019a; Zhang et al., 2020b). The HC obtained from the microwave-assisted HTC of SS with CaO as a catalyst may be a promising bio-fertilizer, which possesses alkaline properties and a lower content of soluble N/P/K and available heavy metals. As mentioned in Sections 3.5.2 and 3.5.3, the microwave-assisted HTC of SS might be further improved through col-HTC treatment to promote the application potential of HC. Future research must focus on the application of HC formed by microwave-assisted HTC of SS.

4. Conclusions

The microwave-assisted HTC of SS was preliminarily explored in this study. Through the investigation of the yield and properties of HC and PW, the following conclusions can be drawn:

- (1) The yield of HC decreased with increasing reaction temperature and time, and increased with increasing solid-liquid ratio. The addition of CaO as a catalyst further promoted the yield of HC, whereas it was reduced in the case of H₃PO₄.
- (2) Compared with the raw SS feedstock, the HC exhibited higher aromaticity, carbonization degree, porosity, and polarity, suggesting its higher application potential for land use and adsorbent. However, the lower caloric value and poor combustion performance of HC limited its application as an energy source.
- (3) The main nutrients (N/P/K) were immobilized in HCs, reducing the risk of loss of nutrients. CaO as a catalyst further promoted the recovery of P and K in HC. H₃PO₄ as a catalyst led to a high P content in the HC and PW.

- (4) All six heavy metals investigated were enriched in HCs; thus, the total contents of Cd and Ni exceeded the standard value for use in cultivated land with edible crops, but the leachable content of heavy metals decreased. When H₃PO₄ was used as the catalyst, it reduced the total content of Zn and Cd in HC, but increased the leachable content of these two heavy metals. For reducing the risk of heavy metal pollution during the land use of HC, the col-HTC of SS and other biomass with low heavy metal content is suggested.
- (5) The PW still contained a high content of organic matter and nutrients, which could be further recovered through some processes, such as anaerobic digestion, algal cultivation, and supercritical water gasification.

CRedit authorship contribution statement

Yu-jie Wang: Writing – original draft, Validation. **Yi Yu:** Investigation, Resources. **Hua-jun Huang:** Conceptualization, Methodology, Writing – review & editing. **Cheng-long Yu:** Software. **Han-sun Fang:** Supervision, Project administration. **Chun-huo Zhou:** Formal analysis, Data curation, Visualization. **Xin Yin:** Investigation, Resources. **Wei-hua Chen:** Investigation, Resources. **Xin-chun Guo:** Writing – review & editing.

Declaration of competing interest

The authors declare that they have no known competing financial interests or personal relationships that could have appeared to influence the work reported in this paper.

Acknowledgments

The authors gratefully acknowledge the financial support provided by the National Natural Science Foundation of China (No. 21707056) and the Natural Science Foundation of Jiangxi Province, China (20192BAB203019).

Appendix A. Supplementary data

Supplementary data to this article can be found online at <https://doi.org/10.1016/j.scitotenv.2021.149874>.

References

- Arpia, A.A., Chen, W.H., Lam, S.S., Rousset, P., de Luna, M.D.G., 2021. Sustainable biofuel and bioenergy production from biomass waste residues using microwave-assisted heating: a comprehensive review. *Chem. Eng. J.* 403, 126233. <https://doi.org/10.1016/j.cej.2020.126233>.
- Aragón-Briceño, C.I., Grasham, O., Ross, A.B., Dupont, V., Camargo-Valero, M.A., 2020. Hydrothermal carbonization of sewage digestate at wastewater treatment works: influence of solid loading on characteristics of hydrochar, process water and plant energetics. *Renew. Energ.* 157, 959–973. <https://doi.org/10.1016/j.renene.2020.05.021>.
- Bach, Q.V., Chen, W.H., Lin, S.C., Sheen, H.K., Chang, J.S., 2017. Wet torrefaction of microalga *Chlorella vulgaris* ESP-31 with microwave-assisted heating. *Energ. Convers. Manag.* 141, 163–170. <https://doi.org/10.1016/j.enconman.2016.07.035>.
- Bao, S.D., 2000. *Soil Agrochemical Analysis*. China Agricultural Publishing House, Beijing, China, pp. 56–58.
- Billar, P., Friedman, C., Ross, A.B., 2013. Hydrothermal microwave processing of microalgae as a pre-treatment and extraction technique for bio-fuels and bio-products. *Bioresour. Technol.* 136, 188–195. <https://doi.org/10.1016/j.biortech.2013.02.088>.
- Cao, L., Yu, I.K.M., Cho, D.-W., Wang, D., Tsang, D.C.W., Zhang, S., Ding, S., Wang, L., Ok, Y.S., 2019. Microwave-assisted low-temperature hydrothermal treatment of red seaweed (*Gracilaria lemaneiformis*) for production of levulinic acid and algae hydrochar. *Bioresour. Technol.* 273, 251–258. <https://doi.org/10.1016/j.biortech.2018.11.013>.
- Chanaka Udayanga, W.D., Veksha, A., Giannis, A., Lisak, G., Chang, V.W.C., Lim, T.T., 2018. Fate and distribution of heavy metals during thermal processing of sewage sludge. *Fuel* 226, 721–744. <https://doi.org/10.1016/j.fuel.2018.04.045>.
- Chang, Z., Long, G., Zhou, J.L., Ma, C., 2020. Valorization of sewage sludge in the fabrication of construction and building materials: a review. *Resour. Conserv. Recy.* 154, 104606. <https://doi.org/10.1016/j.resconrec.2019.104606>.
- Chu, Q., Xue, L., Singh, B.P., Yu, S., Müller, K., Wang, H., Feng, Y., Pan, G., Zheng, X., Yang, L., 2020. Sewage sludge-derived hydrochar that inhibits ammonia volatilization, improves soil nitrogen retention and rice nitrogen utilization. *Chemosphere* 245, 125558. <https://doi.org/10.1016/j.chemosphere.2019.125558>.
- Chung, J., Edewi, O., Foppen, J., Gerner, G., Krebs, R., Lens, P., 2017. Removal of *Escherichia coli* by intermittent operation of saturated sand columns supplemented with hydrochar derived from sewage sludge. *Appl. Sci.-Basel*. 7 (8), 839. <https://doi.org/10.3390/app7080839>.
- Deng, Y., Zhang, T., Clark, J., Aminabhavi, T., Kruse, A., Tsang, D.C.W., Sharma, B., Zhang, F., Ren, H., 2020. Mechanisms and modelling of phosphorus solid-liquid transformation during the hydrothermal processing of swine manure. *Green Chem.* 22, 5628–5638. <https://doi.org/10.1039/D0GC01281E>.
- Elaiwu, S.E., Greenway, G.M., 2016. Microwave-assisted hydrothermal carbonization of rapeseed husk: a strategy for improving its solid fuel properties. *Fuel Process. Technol.* 149, 305–312. <https://doi.org/10.1016/j.fuproc.2016.04.030>.
- Fonts, I., Gea, G., Azuara, M., Abrego, J., Arauzo, J., 2012. Sewage sludge pyrolysis for liquid production: a review. *Renew. Sust. Energ. Rev.* 16 (5), 2781–2805. <https://doi.org/10.1016/j.rser.2012.02.070>.
- Fu, Q., Wang, D., Li, X., Yang, Q., Xu, Q., Ni, B.-J., Wang, Q., Liu, X., 2021. Towards hydrogen production from waste activated sludge: principles, challenges and perspectives. *Renew. Sust. Energ. Rev.* 135, 110283. <https://doi.org/10.1016/j.rser.2020.110283>.
- Gan, Y.Y., Ong, H.C., Chen, W.H., Sheen, H.K., Chang, J.S., Chong, C.T., Ling, T.C., 2020. Microwave-assisted wet torrefaction of microalgae under various acids for coproduction of biochar and sugar. *J. Clean. Prod.* 253, 119944. <https://doi.org/10.1016/j.jclepro.2019.119944>.
- Gao, N., Kamran, K., Quan, C., Williams, P.T., 2020. Thermochemical conversion of sewage sludge: a critical review. *Prog. Energ. Combust.* 79, 100843. <https://doi.org/10.1016/j.pecs.2020.100843>.
- Gao, Y., Liu, Y., Zhu, G., Xu, J., Xu, H., Yuan, Q., Zhu, Y., Sarma, J., Wang, Y., Wang, J., Ji, L., 2018. Microwave-assisted hydrothermal carbonization of dairy manure: chemical and structural properties of the products. *Energy* 165, 662–672. <https://doi.org/10.1016/j.energy.2018.09.185>.
- Gaur, R.Z., Khoury, O., Zohar, M., Poverenov, E., Darzi, R., Laor, Y., Posmanik, R., 2020. Hydrothermal carbonization of sewage sludge coupled with anaerobic digestion: integrated approach for sludge management and energy recycling. *Energ. Convers. Manag.* 224, 113353. <https://doi.org/10.1016/j.enconman.2020.113353>.
- Hämäläinen, A., Kokko, M., Kinnunen, V., Hilli, T., Rintala, J., 2021. Hydrothermal carbonisation of mechanically dewatered digested sewage sludge—Energy and nutrient recovery in centralised biogas plant. *Water Res.* 201, 117284. <https://doi.org/10.1016/j.watres.2021.117284>.
- He, C., Giannis, A., Wang, J.-Y., 2013. Conversion of sewage sludge to clean solid fuel using hydrothermal carbonization: hydrochar fuel characteristics and combustion behavior. *Appl. Energ.* 111, 257–266. <https://doi.org/10.1016/j.apenergy.2013.04.084>.
- He, C., Zhang, Z., Ge, C., Liu, W., Tang, Y., Zhuang, X., Qiu, R., 2019. Synergistic effect of hydrothermal co-carbonization of sewage sludge with fruit and agricultural wastes on hydrochar fuel quality and combustion behavior. *Waste Manag.* 100, 171–181. <https://doi.org/10.1016/j.wasman.2019.09.018>.
- Heilmann, S.M., Molde, J.S., Timler, J.G., Wood, B.M., Mikula, A.L., Vozhdayev, G.V., Colosky, E.C., Spokas, K.A., Valentas, K.J., 2014. Phosphorus reclamation through hydrothermal carbonization of animal manures. *Environ. Sci. Technol.* 48 (17), 10323–10329. <https://doi.org/10.1021/es501872k>.
- Hosokai, S., Matsuoka, K., Kuramoto, K., Suzuki, Y., 2016. Modification of Dulong's formula to estimate heating value of gas, liquid and solid fuels. *Fuel Process. Technol.* 152, 399–405. <https://doi.org/10.1016/j.fuproc.2016.06.040>.
- Huang, H.J., Chang, Y.C., Lai, F.Y., Zhou, C.F., Pan, Z.Q., Xiao, X.F., Wang, J.X., Zhou, C.H., 2019. Co-liquefaction of sewage sludge and rice straw/wood sawdust: the effect of process parameters on the yields/properties of bio-oil and biochar products. *Energy* 173, 140–150. <https://doi.org/10.1016/j.energy.2019.02.071>.
- Huang, H.J., Yang, T., Lai, F.Y., Wu, G.Q., 2017. Co-pyrolysis of sewage sludge and sawdust/rice straw for the production of biochar. *J. Anal. Appl. Pyrol.* 125 (Supplement C), 61–68. <https://doi.org/10.1016/j.jaap.2017.04.018>.
- Huang, H.J., Yuan, X.Z., 2016. The migration and transformation behaviors of heavy metals during the hydrothermal treatment of sewage sludge. *Bioresour. Technol.* 200, 991–998. <https://doi.org/10.1016/j.biortech.2015.10.099>.
- Huang, H.J., Yuan, X.Z., 2015. Recent progress in the direct liquefaction of typical biomass. *Prog. Energ. Combust.* 49, 59–80. <https://doi.org/10.1016/j.pecs.2015.01.003>.
- Huang, R., Zhang, B., Saad, E.M., Ingall, E.D., Tang, Y., 2018. Speciation evolution of zinc and copper during pyrolysis and hydrothermal carbonization treatments of sewage sludges. *Water Res.* 132, 260–269. <https://doi.org/10.1016/j.watres.2018.01.009>.
- Jin, H., Yan, D., Zhu, N., Zhang, S., Zheng, M., 2019. Immobilization of metal(loid)s in hydrochars produced from digested swine and dairy manures. *Waste Manag.* 88, 10–20. <https://doi.org/10.1016/j.wasman.2019.03.027>.
- Kang, K., Nanda, S., Sun, G., Qiu, L., Gu, Y., Zhang, T., Zhu, M., Sun, R., 2019. Microwave-assisted hydrothermal carbonization of corn stalk for solid biofuel production: optimization of process parameters and characterization of hydrochar. *Energy* 186, 115795. <https://doi.org/10.1016/j.energy.2019.07.125>.
- Knappe, V., Paczkowski, S., Tejada, J., Diaz Robles, L.A., Gonzalez, A., Pelz, S., 2018. Low temperature microwave assisted hydrothermal carbonization (MAHC) reduces combustion emission precursors in short rotation coppice willow wood. *J. Anal. Appl. Pyrol.* 134, 162–166. <https://doi.org/10.1016/j.jaap.2018.06.004>.
- Lai, F.Y., Chang, Y.C., Huang, H.J., Wu, G.Q., Xiong, J.B., Pan, Z.Q., Zhou, C.F., 2018. Liquefaction of sewage sludge in ethanol-water mixed solvents for bio-oil and biochar products. *Energy*. <https://doi.org/10.1016/j.energy.2018.01.186>.
- Lang, Q., Luo, H., Li, Y., Li, D., Liu, Z., Yang, T., 2019a. Thermal behavior of hydrochar from co-hydrothermal carbonization of swine manure and sawdust: effect of process water recirculation. *Sustain. Energ. Fuels*. <https://doi.org/10.1039/C9SE00332K>.
- Lang, Q., Zhang, B., Liu, Z., Jiao, W., Xia, Y., Chen, Z., Li, D., Ma, J., Gai, C., 2019b. Properties of hydrochars derived from swine manure by CaO assisted hydrothermal carbonization. *J. Environ. Manag.* 233, 440–446. <https://doi.org/10.1016/j.jenvman.2018.12.072>.
- Lang, Q., Zhang, B., Liu, Z., Chen, Z., Xia, Y., Li, D., Ma, J., Gai, C., 2019c. Co-hydrothermal carbonization of corn stalk and swine manure: combustion behavior of hydrochar by thermogravimetric analysis. *Bioresour. Technol.* 271 (2019), 75–83.
- Leng, L., Yang, L., Chen, J., Hu, Y., Li, H., Li, H., Jiang, S., Peng, H., Yuan, X., Huang, H., 2021. Valorization of the aqueous phase produced from wet and dry thermochemical processing biomass: a review. *J. Clean. Prod.* 294, 126238. <https://doi.org/10.1016/j.jclepro.2021.126238>.
- Leng, L., Zhang, W., Leng, S., Chen, J., Yang, L., Li, H., Jiang, S., Huang, H., 2020. Bioenergy recovery from wastewater produced by hydrothermal processing biomass: Progress, challenges, and opportunities. *Sci. Total Environ.* 748, 142383. <https://doi.org/10.1016/j.scitotenv.2020.142383>.
- Liu, H., Basar, I.A., Nzihou, A., Eskicioglu, C., 2021a. Hydrochar derived from municipal sludge through hydrothermal processing: a critical review on its formation, characterization, and valorization. *Water Res.* 199, 117186. <https://doi.org/10.1016/j.watres.2021.117186>.
- Liu, J., Zhong, F., Niu, W., Zhao, Y., Su, J., Feng, Y., Meng, H., 2021c. Effects of temperature and catalytic methods on the physicochemical properties of microwave-assisted hydrothermal products of crop residues. *J. Clean. Prod.* 279, 123512. <https://doi.org/10.1016/j.jclepro.2020.123512>.
- Liu, T., Liu, Z., Zheng, Q., Lang, Q., Xia, Y., Peng, N., Gai, C., 2018. Effect of hydrothermal carbonization on migration and environmental risk of heavy metals in sewage sludge during pyrolysis. *Bioresour. Technol.* 247, 282–290. <https://doi.org/10.1016/j.biortech.2017.09.090>.
- Liu, T., Tian, L., Liu, Z., He, J., Fu, H., Huang, Q., Xue, H., Huang, Z., 2021b. Distribution and toxicity of polycyclic aromatic hydrocarbons during CaO-assisted hydrothermal carbonization of sewage sludge. *Waste Manag.* 120, 616–625. <https://doi.org/10.1016/j.wasman.2020.10.025>.
- Liu, Y., Sun, Y., Wan, Z., Jing, F., Li, Z., Chen, J., Tsang, D.C.W., 2021d. Tailored design of food waste hydrochar for efficient adsorption and catalytic degradation of refractory organic contaminant. *J. Clean. Prod.* 310, 127482. <https://doi.org/10.1016/j.jclepro.2021.127482>.
- Lu, X., Ma, X., Qin, Z., Chen, X., Chen, L., Tian, Y., 2021. Co-hydrothermal carbonization of sewage sludge and polyvinyl chloride: hydrochar properties and fate of chlorine and heavy metals. *J. Environ. Chem. Eng.* 9 (5), 106143. <https://doi.org/10.1016/j.jece.2021.106143>.
- Malhotra, M., Garg, A., 2020. Hydrothermal carbonization of centrifuged sewage sludge: determination of resource recovery from liquid fraction and thermal behaviour of hydrochar. *Waste Manag.* 117, 114–123. <https://doi.org/10.1016/j.wasman.2020.07.026>.
- Manara, P., Zabaniotou, A., 2012. Towards sewage sludge based biofuels via thermochemical conversion – a review. *Renew. Sust. Energ. Rev.* 16 (5), 2566–2582. <https://doi.org/10.1016/j.rser.2012.01.074>.
- Ministry of Housing and Urban-Rural Development of the People's Republic of China (M, HURD of China), 2020. *Statistical Yearbook of Urban and Rural Construction in China (2019)*. China Statistical Publishing House.
- Ministry of Housing and Urban-Rural Development of the People's Republic of China (MOHURD), 2005. *Determination method for municipal sludge in wastewater treatment plant*. Industrial Standard of Urban Construction of the People's Republic of China, CJ/T. 221.
- Ministry of Ecology and Environment of the People's Republic of China, 2014. *Soil quality-Determination of available phosphorus-Sodium hydrogen carbonate-Mo-Sb anti spectrophotometric method*. Environmental Protection Standards of the People's Republic of China, HJ. 704.

- Ministry of Agricultural and Rural Affairs of the People's Republic of China, 2004. Determination of exchangeable potassium and non-exchangeable potassium content in soil. Agricultural Industry Standard of the People's Republic of China, NY/T. 889.
- Ministry of Ecology and Environment of the People's Republic of China, 2009. Water quality—Determination of ammonia nitrogen—Nessler's reagent spectrophotometry. Environmental Protection Standards of the People's Republic of China, HJ. 535.
- Nizamuddin, S., Baloch, H.A., Griffin, G.J., Mubarak, N.M., Bhutto, A.W., Abro, R., Mazari, S.A., Ali, B.S., 2017. An overview of effect of process parameters on hydrothermal carbonization of biomass. *Renew. Sust. Energ. Rev.* 73, 1289–1299. <https://doi.org/10.1016/j.rser.2016.12.122>.
- Nizamuddin, S., Baloch, H.A., Siddiqui, M.T.H., Mubarak, N.M., Tunio, M.M., Bhutto, A.W., Jatoi, A.S., Griffin, G.J., Srinivasan, M.P., 2018. An overview of microwave hydrothermal carbonization and microwave pyrolysis of biomass. *Rev. Environ. Sci. Bio.* 17 (4), 813–837. <https://doi.org/10.1007/s1157-018-9476-z>.
- Pan, Z.Q., Huang, H.J., Zhou, C.F., Lai, F.Y., He, X.W., Xiong, J.B., Xiao, X.F., 2019. Distribution and transformation behaviors of heavy metals during the liquefaction process of sewage sludge in ethanol-water mixed solvents. *J. Cent. South Univ.* <https://doi.org/10.1007/s11771-019-4212-6>.
- Pan, Z.Q., Huang, H.J., Zhou, C.F., Xiao, X.F., He, X.W., Lai, F.Y., Xiong, J.B., 2018. Highly efficient conversion of camphor tree sawdust into bio-oil and biochar products by liquefaction in ethanol-water cosolvent. *J. Anal. Appl. Pyrol.* 136, 186–198. <https://doi.org/10.1016/j.jaap.2018.10.006>.
- Paneque, M., De la Rosa, J.M., Kern, J., Reza, M.T., Knicker, H., 2017. Hydrothermal carbonization and pyrolysis of sewage sludges: what happen to carbon and nitrogen? *J. Anal. Appl. Pyrol.* 128, 314–323. <https://doi.org/10.1016/j.jaap.2017.09.019>.
- Peng, C., Zhai, Y., Zhu, Y., Xu, B., Wang, T., Li, C., Zeng, G., 2016. Production of char from sewage sludge employing hydrothermal carbonization: char properties, combustion behavior and thermal characteristics. *Fuel* 176, 110–118. <https://doi.org/10.1016/j.fuel.2016.02.068>.
- Ren, J., Wang, F., Zhai, Y., Zhu, Y., Peng, C., Wang, T., Li, C., Zeng, G., 2017. Effect of sewage sludge hydrochar on soil properties and cd immobilization in a contaminated soil. *Chemosphere* 189, 627–633. <https://doi.org/10.1016/j.chemosphere.2017.09.102>.
- Shao, Y., Tan, H., Shen, D., Zhou, Y., Jin, Z., Zhou, D., Lu, W., Long, Y., 2020. Synthesis of improved hydrochar by microwave hydrothermal carbonization of green waste. *Fuel* 266, 117146. <https://doi.org/10.1016/j.fuel.2020.117146>.
- Sharma, H.B., Sarmah, A.K., Dubej, B., 2020. Hydrothermal carbonization of renewable waste biomass for solid biofuel production: a discussion on process mechanism, the influence of process parameters, environmental performance and fuel properties of hydrochar. *Renew. Sust. Energ. Rev.* 123, 109761. <https://doi.org/10.1016/j.rser.2020.109761>.
- Shen, Y., 2020. A review on hydrothermal carbonization of biomass and plastic wastes to energy products. *Biomass Bioenerg.* 134, 105479. <https://doi.org/10.1016/j.biombioe.2020.105479>.
- Shi, W., Liu, C., Shu, Y., Feng, C., Lei, Z., Zhang, Z., 2013. Synergistic effect of rice husk addition on hydrothermal treatment of sewage sludge: fate and environmental risk of heavy metals. *Bioresour. Technol.* 149, 496–502. <https://doi.org/10.1016/j.biortech.2013.09.114>.
- Sing, K.S.W., Everett, D.H., Haul, R.A.W., Moscou, L., Pierotti, R.A., Rouquerol, J., Siemieniowska, T., 1985. Reporting physisorption data for gas/solid systems with special reference to the determination of surface area and porosity. *Pure Appl. Chem.* 57 (4), 7. <https://doi.org/10.1351/pac198557040603>.
- Syed-Hassan, S.S.A., Wang, Y., Hu, S., Su, S., Xiang, J., 2017. Thermochemical processing of sewage sludge to energy and fuel: fundamentals, challenges and considerations. *Renew. Sust. Energ. Rev.* 80, 888–913. <https://doi.org/10.1016/j.rser.2017.05.262>.
- Tarpani, R.R.Z., Alfonsín, C., Hospido, A., Azapagic, A., 2020. Life cycle environmental impacts of sewage sludge treatment methods for resource recovery considering ecotoxicity of heavy metals and pharmaceutical and personal care products. *J. Environ. Manag.* 260, 109643. <https://doi.org/10.1016/j.jenvman.2019.109643>.
- Tasca, A.L., Puccini, M., Gori, R., Corsi, I., Galletti, A.M.R., Vitolo, S., 2019. Hydrothermal carbonization of sewage sludge: a critical analysis of process severity, hydrochar properties and environmental implications. *Waste Manag.* 93, 1–13. <https://doi.org/10.1016/j.wasman.2019.05.027>.
- Tasca, A.L., Puccini, M., Stefanelli, E., Gori, R., Galletti, A.M.R., Vitolo, S., 2020. Investigating the activation of hydrochar from sewage sludge for the removal of terbuthylazine from aqueous solutions. *J. Mater. Cycles Waste.* 22 (5), 1539–1551. <https://doi.org/10.1007/s10163-020-01045-y>.
- Usman, M., Chen, H., Chen, K., Ren, S., Clark, J.H., Fan, J., Luo, G., Zhang, S., 2019. Characterization and utilization of aqueous products from hydrothermal conversion of biomass for bio-oil and hydro-char production: a review. *Green Chem.* 21, 1553–1572. <https://doi.org/10.1039/C8CC03957G>.
- Wang, C., Zhu, W., Fan, X., 2021. Char derived from sewage sludge of hydrothermal carbonization and supercritical water gasification: comparison of the properties of two chars. *Waste Manag.* 123, 88–96. <https://doi.org/10.1016/j.wasman.2021.01.027>.
- Wang, J.X., Chen, S.W., Lai, F.Y., Liu, S.Y., Xiong, J.B., Zhou, C.F., Yi, Y., Huang, H.J., 2020a. Microwave-assisted hydrothermal carbonization of pig feces for the production of hydrochar. *J. Supercrit. Fluid.* 162, 104858. <https://doi.org/10.1016/j.supflu.2020.104858>.
- Wang, J.X., Liu, P., Lai, F.Y., Huang, H.J., 2020b. Pyrolysis of different sewage sludge feedstocks for biochar products: characterization and application. *J. Cent. South Univ.* 27 (11), 3302–3319. <https://doi.org/10.1007/s11771-020-4548-y>.
- Wang, L., Chang, Y., Li, A., 2019a. Hydrothermal carbonization for energy-efficient processing of sewage sludge: a review. *Renew. Sust. Energ. Rev.* 108, 423–440. <https://doi.org/10.1016/j.rser.2019.04.011>.
- Wang, L., Chang, Y., Liu, Q., 2019b. Fate and distribution of nutrients and heavy metals during hydrothermal carbonization of sewage sludge with implication to land application. *J. Clean. Prod.* 225, 972–983. <https://doi.org/10.1016/j.jclepro.2019.03.347>.
- Wang, L., Chang, Y., Zhang, X., Yang, F., Li, Y., Yang, X., Dong, S., 2020c. Hydrothermal co-carbonization of sewage sludge and high concentration phenolic wastewater for production of solid biofuel with increased calorific value. *J. Clean. Prod.* 255, 120317. <https://doi.org/10.1016/j.jclepro.2020.120317>.
- Wang, S., Persson, H., Yang, W., Jönsson, P.G., 2020d. Pyrolysis study of hydrothermal carbonization-treated digested sewage sludge using a py-CG/MS and a bench-scale pyrolyzer. *Fuel* 262, 116335. <https://doi.org/10.1016/j.fuel.2019.116335>.
- Wilk, M., Magdziarz, A., Jayaraman, K., Szymanska-Chargot, M., Gökalp, I., 2019. Hydrothermal carbonization characteristics of sewage sludge and lignocellulosic biomass. A comparative study. *Biomass Bioenerg.* 120, 166–175. <https://doi.org/10.1016/j.biombioe.2018.11.016>.
- Wilk, M., Sliz, M., Lubieniecki, B., 2021. Hydrothermal co-carbonization of sewage sludge and fuel additives: combustion performance of hydrochar. *Renew. Energ.* 178, 1046–1056. <https://doi.org/10.1016/j.renene.2021.06.101>.
- Xiao, X.F., Chang, Y.C., Lai, F.Y., Fang, H.S., Zhou, C.F., Pan, Z.Q., Wang, J.X., Wang, Y.J., Yin, X., Huang, H.J., 2020. Effects of rice straw/wood sawdust addition on the transport/conversion behaviors of heavy metals during the liquefaction of sewage sludge. *J. Environ. Manag.* 270, 110824. <https://doi.org/10.1016/j.jenvman.2020.110824>.
- Xiong, J.B., Pan, Z.Q., Xiao, X.F., Huang, H.J., Lai, F.Y., Wang, J.X., Chen, S.W., 2019. Study on the hydrothermal carbonization of swine manure: the effect of process parameters on the yield/properties of hydrochar and process water. *J. Anal. Appl. Pyrol.* 144, 104692. <https://doi.org/10.1016/j.jaap.2019.104692>.
- Xu, X., Jiang, E., 2017. Treatment of urban sludge by hydrothermal carbonization. *Bioresour. Technol.* 238, 182–187. <https://doi.org/10.1016/j.biortech.2017.03.174>.
- Yang, T., Huang, H.J., Lai, F.Y., 2017. Pollution hazards of heavy metals in sewage sludge from four wastewater treatment plants in Nanchang, China. *T. Nonfer. Metal. Soc.* 27 (10), 2249–2259. [https://doi.org/10.1016/S1003-6326\(17\)60251-6](https://doi.org/10.1016/S1003-6326(17)60251-6).
- Yu, I.K.M., Fan, J., Budarin, V., Bouxin, F., Clark, J., Tsang, D.C.W., 2020b. Evidences of starch-microwave interactions under hydrolytic and pyrolytic conditions. *Green Chem.* 22, 7109–7118. <https://doi.org/10.1039/D0GC02644A>.
- Yu, K.L., Chen, W.H., Sheen, H.K., Chang, J.S., Lin, C.S., Ong, H.C., Show, P.L., Ng, E.P., Ling, T.C., 2020a. Production of microalgal biochar and reducing sugar using wet torrefaction with microwave-assisted heating and acid hydrolysis pretreatment. *Renew. Energ.* 156, 349–360. <https://doi.org/10.1016/j.renene.2020.04.064>.
- Yu, Y., Lei, Z., Yang, X., Yang, X., Huang, W., Shimizu, K., Zhang, Z., 2018. Hydrothermal carbonization of anaerobic granular sludge: effect of process temperature on nutrients availability and energy gain from produced hydrochar. *Appl. Energ.* 229, 88–95. <https://doi.org/10.1016/j.apenergy.2018.07.088>.
- Yuan, X., Huang, H., Zeng, G., Li, H., Wang, J., Zhou, C., Zhu, H., Pei, X., Liu, Z., Liu, Z., 2011. Total concentrations and chemical speciation of heavy metals in liquefaction residues of sewage sludge. *Bioresour. Technol.* 102 (5), 4104–4110. <https://doi.org/10.1016/j.biortech.2010.12.055>.
- Zhai, Y., Liu, X., Zhu, Y., Peng, C., Wang, T., Zhu, L., Li, C., Zeng, G., 2016. Hydrothermal carbonization of sewage sludge: the effect of feed-water pH on fate and risk of heavy metals in hydrochars. *Bioresour. Technol.* 218, 183–188. <https://doi.org/10.1016/j.biortech.2016.06.085>.
- Zhang, H., Xue, G., Chen, H., Li, X., Chen, S., 2021a. Revealing the heating value characteristics of sludge-based hydrochar in hydrothermal process: from perspective of hydrolysis. *Water Res.* 198, 117170. <https://doi.org/10.1016/j.watres.2021.117170>.
- Zhang, K., Zhang, K., Cao, Y., Pan, W.P., 2013. Co-combustion characteristics and blending optimization of tobacco stem and high-sulfur bituminous coal based on thermogravimetric and mass spectrometry analyses. *Bioresour. Technol.* 131, 325–332. <https://doi.org/10.1016/j.biortech.2012.12.163>.
- Zhang, S., Pi, M., Su, Y., Xu, D., Xiong, Y., Zhang, H., 2020a. Physicochemical properties and pyrolysis behavior evaluations of hydrochar from co-hydrothermal treatment of rice straw and sewage sludge. *Biomass. Bioenerg.* 140, 105664. <https://doi.org/10.1016/j.biombioe.2020.105664>.
- Zhang, T., He, X., Deng, Y., Tsang, D.C.W., Yuan, H., Shen, J., Zhang, S., 2020b. Swine manure valorization for phosphorus and nitrogen recovery by catalytic-thermal hydrolysis and struvite crystallization. *Sci. Total Environ.* 729, 138999. <https://doi.org/10.1016/j.scitotenv.2020.138999>.
- Zhang, X., Zhang, L., Li, A., 2017. Hydrothermal co-carbonization of sewage sludge and pinewood sawdust for nutrient-rich hydrochar production: synergistic effects and products characterization. *J. Environ. Manag.* 201, 52–62. <https://doi.org/10.1016/j.jenvman.2017.06.018>.
- Zhang, Y., Deng, Q., Wang, M., Zhang, J., Man, Y.B., Shan, S., Wu, S., Liang, P., Cao, Y., Song, C., Luo, L., Lin, L., Christie, P., Wong, M.H., 2018. Role of phosphoric acid in the bio-availability of potentially toxic elements in hydrochars produced by hydrothermal carbonisation of sewage sludge. *Waste Manag.* 79, 232–239. <https://doi.org/10.1016/j.wasman.2018.07.045>.
- Zhang, Y., Qin, J., Yi, Y., 2021b. Biochar and hydrochar derived from freshwater sludge: characterization and possible applications. *Sci. Total Environ.* 763, 144550. <https://doi.org/10.1016/j.scitotenv.2020.144550>.
- Zhang, Y., Zahid, I., Danial, A., Minaret, J., Cao, Y., Dutta, A., 2021c. Hydrothermal carbonization of miscanthus: processing, properties, and synergistic co-combustion with lignite. *Energy* 225, 120200. <https://doi.org/10.1016/j.energy.2021.120200>.
- Zheng, X., Huang, J., Ying, Z., Ji, S., Feng, Y., Wang, B., Dou, B., 2021. Thermochemical conversion of sewage sludge-derived hydrochars: volatiles release and char gasification kinetics. *J. Anal. Appl. Pyrol.* 156, 105138. <https://doi.org/10.1016/j.jaap.2021.105138>.